Cosmic microwave background anisotropies from pre-big bang cosmology

F. Vernizzi,[1] A. Melchiorri,[1,2,3] and R. Durrer[1]

[1]*Département de Physique Théorique, Université de Genève, 24 quai E. Ansermet, 1211 Genève 4, Switzerland*
[2]*Università Tor Vergata, Roma, Italy*
[3]*NAPL, University of Oxford, Keble Road, Oxford OX1 3RH, England*
(Received 16 August 2000; published 5 February 2001)

We present an alternative scenario for cosmic structure formation where initial fluctuations are due to Kalb-Ramond axions produced during a pre-big bang phase of inflation. We investigate whether this scenario, where the fluctuations are induced by seeds and therefore are of isocurvature nature, can be brought in agreement with present observations by a suitable choice of cosmological parameters. We also discuss several observational signatures which can distinguish axion seeds from standard inflationary models. We finally discuss the gravitational wave background induced in this model and we show that it may be well within the range of future observations.

I. INTRODUCTION

It is commonly assumed that an inflationary phase is necessary in order to construct a consistent cosmological model. The familiar adiabatic inflationary scenario owes its popularity to the fact that it solves the horizon and flatness problems and at the same time provides a consistent model for the origin of cosmological perturbations. In particular, it naturally leads to a flat (Harrison–Zel'dovich) spectrum of perturbations on large scale and to coherent acoustic oscillations on intermediate scales which manifest themselves as ''peaks'' in the cosmic microwave background (CMB) anisotropies.

After the recent measurements of the intermediate scale CMB anisotropy power spectrum [1–4], flat adiabatic models seem to be favored [5–8]. Nevertheless none of the many inflationary scenarios which have been developed during the last 20 years has been constructed consistently on the bases of a serious theory of high energy physics; inflation has always been seen as an effective model pointing to a greater more fundamental theory which has not been clarified so far. We believe that superstrings are presently the most promising candidate for such a theory but on the other hand it is well known that it is not possible to derive an inflationary model from a string theory effective action on a generic background, the reason being that the nonminimal coupling between the dilaton and the metric slows down the expansion of the universe spoiling the solution of the problems for which inflation has been invoked.

The pre-big bang idea [9] represents in this context one of the first and most interesting attempts to develop a new cosmological scenario which solves the horizon and flatness problems, based on string theory. In this radically new picture, the underlying duality symmetry [10] present in the low energy sector of string theory naturally selects perturbative initial conditions and automatically leads to an inflationary phase prior to the big bang during which curvature and the dilaton are growing [9,11]. Besides its many appealing features, this scenario is known to face several problems such as the lack of a complete and consistent description of the high coupling and high curvature regime where the transition be-

tween the pre-big bang and the post-big bang phase and the stabilization of the dilaton should take place [12]. Furthermore, opinions vary as to whether the initial conditions in the pre-big bang need a large amount of fine tuning [11,13]. On a more phenomenological side, it is nevertheless important to study whether this scenario can provide the features that we observe in the universe today. For recent review papers discussing several of the previous points we refer the reader to Refs. [14,15]. For a comparison of the pre-big bang model with new cosmological models based on string theory see Ref. [16].

A realistic cosmological model has to generate large-scale matter perturbations and to reproduce the slope and the amplitude of CMB anisotropy spectrum. The pre-big bang scenario was thought for some time to be unable to provide a scale-invariant spectrum of perturbations. First-order tensor and scalar perturbations in the metric, as well as perturbations of the moduli fields, were found to be characterized by extremely ''blue'' spectra [17]. This large tilt, together with a natural normalization imposed by the string cutoff at the shortest amplified scales, make their contribution to large-scale structure completely negligible.

However, it was later realized that the spectral tilt of the axion, a universal field in string theory, can assume a whole range of values depending on the behavior of the internal and external dimensions and in particular it can naturally provide a scale-invariant spectrum of perturbations [18–20]. This result reopened the possibility that pre-big bang cosmology may contain a natural mechanism for generating large-scale CMB anisotropies via the ''seed'' mechanism [21].

This possibility was analyzed in Refs. [22,23] for massless axions and in Ref. [24] for very light axions. These analytical treatments are restricted to large angular scales. We have extended the study to smaller scales with the help of numerical calculations. First results of this work have been reported in a letter [25], where a strong correlation between the axion spectrum, n_σ, and the height of the peak was noticed. A range of values around $n_\sigma = 1.4$ (slightly blue spectra) appeared to be favored by a simultaneous fit to the normalization on large angular scales observed by the cos-

mic background explorer (COBE) [26] and the data on the first acoustic peak available at that time.

In this companion paper we present a full explanation of the details of these calculations for the CMB angular power spectrum and for the dark matter power spectrum and we study the problem of the ''decoherence'' of axion perturbations which has been ignored in the previous work. Furthermore, we expand on the results for the observational signatures presented in Ref. [25] and we discuss them in the light of the new CMB anisotropy data presently available by investigating the cosmological parameter space of the model. We also discuss CMB polarization for our model and the contribution of the gravitational wave background induced by axion perturbations.

We will suppose for the rest of this work that modes with frequencies relevant to CMB physics are unaffected by the transition from the pre- to the post-big bang phase. This may seem a strong assumption given our ignorance on the graceful exit and on the duration of the intermediate string phase. Indeed, the nature and features of the transition are still unknown and may lead to important changes on the characteristics of the axions spectrum, but we are confident that this can only affect scales much smaller than those we are interested in: For this to hold, we just need that, at the moment we enter the string phase, the CMB modes are well outside the horizon and therefore not altered by any causal process. As shown in Ref. [27] using general arguments, the long-wavelength part of the solution to the equation of motion of the axion field is always dominated by the contribution of the frozen modes even if the background evolution includes a high-curvature phase in which the action and the perturbation equations are not known. This argument has been tested by numerical examples in Ref. [28] for a gravitational wave background spectrum. Recently a graceful exit model considering general high-curvature and coupling corrections has appeared in the literature [29] and numerical tests on the axion spectrum have been performed and will be published soon [30] to confirm our assumption.

The paper is organized as follows: in the next section we study axion production in the pre-big bang and explain the details of the computation of the axion energy-momentum tensor which plays the role of the ''seed'' in our model. In Sec. III we determine the CMB anisotropy and dark matter spectra. We study the problem of decoherence and show that the coherent approximation is very good for this model. In Sec. IV we compare our result with CMB and supernova data and present a cosmological parameter estimation for this scenario. We also examine and discuss the normalization and the kink in the axion spectrum which is required to fit observations. Section V is devoted to a novel prediction of axion seeds: the tensor component of their energy-momentum tensor induces a gravity wave background which might be observable. In Sec. VI we summarize our conclusions.

II. AXION SEEDS FROM STRING COSMOLOGY

A. Extra dimensions in string cosmology

The minimal low energy effective action of the NS–NS sector of string theory in the string frame is given by [31]

$$S_{10} = \int d^{10}x \sqrt{|g_{10}|} e^{-\phi_{10}} [R_{10} + (\nabla \phi_{10})^2 - \tfrac{1}{12} H_{10}^2],$$
(2.1)

where we have included the 10-dimensional antisymmetric tensor $H_{\mu\nu\alpha} = \partial_{[\mu} B_{\nu\alpha]}$, but no gauge or fermion fields.

We assume that the 10-dimensional metric can be factorized into a ''large'' four-dimensional part and a ''small'' six-dimensional metric,

$$ds^2 = g_{\mu\nu} dx^\mu dx^\nu + e^{2\beta} \delta_{IJ} dX^I dX^J$$
(2.2)

($\mu, \nu = 0,...,3$ and $I, J = 1,...,6$), where β depends only on time, $\beta = \beta(t)$. If the six-dimensional piece is compactified to a very small radius, the lowest energy Kaluza–Klein modes yield the four-dimensional action [18],

$$S = \int d^4x \sqrt{|g|} e^{-\phi} [R + (\nabla \phi)^2 - 3(\nabla \beta)^2 - \tfrac{1}{2} e^{2\phi} (\nabla \sigma)^2].$$
(2.3)

Here we have introduced the four-dimensional axion field σ defined by

$$H^{\mu\nu\alpha} = e^\phi \epsilon^{\mu\nu\alpha\beta} \nabla_\beta \sigma.$$
(2.4)

The action (2.3) and the definition (2.4) include the four-dimensional dilation field, ϕ, the pseudoscalar axion field, σ, which represents the degrees of freedom of the antisymmetric three tensor field H, and a modulus field, β, which parametrizes the radius, or the ''breathing mode,'' of the six-dimensional internal space. Like the dilaton, also the axion field (not to be confused with the Peccei-Quinn axion) is universal in string theory.

Let us assume a homogeneous dilation background, $\phi = \phi(t)$, and an external four-dimensional spacetime adequately described by a standard, spatially flat FLRW metric with scale factor $a(t)$,

$$g_{\mu\nu} = \text{diag}[-1, a^2(t), a^2(t), a^2(t)].$$
(2.5)

In the following we shall also make use of the metric

$$g_{\mu\nu} = a^2(\eta) \text{diag}[-1, 1, 1, 1],$$
(2.6)

where we have introduced the conformal time η given by $d\eta = dt/a$ (we shall use an overdot to indicate a derivative with respect to conformal time, $\dot{} \equiv \partial/\partial\eta$). With our choice of the external metric, the four-dimensional dilaton is related to the 10-dimensional one by

$$\phi = \phi_{10} - 6\beta.$$
(2.7)

When the axion field is trivial, $\dot{\sigma} = 0$, or its contribution to the global dynamics of the universe is negligible, the equations derived from the action (2.3) are invariant under duality transformations,

$$a(t) \to 1/a(-t), \quad \phi(t) \to \phi(-t) - 6\ln(a(-t)).$$
(2.8)

This invariance (scale factor duality) represents one of the key motivations behind the pre-big bang scenario [9]. The field equations for a, ϕ, and β are solved [9] by the following power laws, known as dilaton-vacuum solutions in the pre-big bang for $\eta < -\eta_1$:

$$a(\eta) = \left(\frac{-\eta}{\eta_1}\right)^{\delta/(1-\delta)}, \quad e^{\beta(\eta)} = \left(\frac{-\eta}{\eta_1}\right)^{\zeta/(1-\delta)},$$

$$e^{\phi(\eta)} = \left(\frac{-\eta}{\eta_1}\right)^{(3\delta-1)/(1-\delta)}, \tag{2.9}$$

where δ and ζ satisfy the Kasner constraint,

$$3\delta^2 + 6\zeta^2 = 1. \tag{2.10}$$

Here $-\eta_1$ is the (conformal) time at which curvature and dilaton become so large that loop corrections from string theory have to be taken into account. It is hoped that these corrections then lead to a radiation dominated Friedman universe with ''frozen'' dilaton at $\eta > \eta_1$.

From these solutions one can see that, during the pre-big bang phase, i.e., for negative conformal time η, a negative δ and a positive ζ are required to make the external three-dimensional space expand and the internal six-dimensional space contract. Therefore δ has to lie in the interval $-1/\sqrt{3} \le \delta < 0$, which leads always to a growing dilaton and growing four-curvature, $R \sim (\dot{a}/a^2)^2 \propto 1/(a\eta)^2 \propto (-\eta)^{-2/(1-\delta)}$.

B. Amplification of axion quantum fluctuations

In this section we briefly review the mechanism for the generation of a primordial quasi-scale-invariant spectrum from the pre-big bang phase and we discuss the dependence of the spectral index on the evolution of the internal and external dimensions of the pre-big bang universe. Using as initial conditions the axion field obtained during the pre-big bang phase, we then analyze its evolution after the big bang in a critical Friedmann–Lemaitre–Robertson–Walker (FLRW) universe with and without cosmological constant, paying particular attention to the frequency modes that enter into the calculation of the CMB anisotropy power spectrum.

As in previous works [22–25] we suppose that the contribution of the axion field to the equations of motion for ϕ, a, and β is negligible and that the evolution of the dilaton, the moduli, and the scale factor are governed by the dilaton-vacuum solutions (2.9). Nevertheless, quantum fluctuations of all the fields are of course present and we will show that quantum fluctuations of the axion field can seed density perturbations and CMB anisotropies in the post-big bang era. To this goal we have to study the axion evolution equation and the spectrum of axions produced during the pre-big bang phase due to their coupling to the background gravitational field and the dilaton.

Varying the action (2.3) with respect to the field σ in the string frame yields the equation of motion

$$\nabla_\mu(e^\phi \nabla^\mu \sigma) = 0. \tag{2.11}$$

The study of this equation is conveniently performed by using the canonical variable given by

$$\psi \equiv a_A \sigma \equiv a e^{\phi/2}\sigma, \tag{2.12}$$

which ''diagonalizes'' the perturbed action expanded up to second order. The factor a_A is the so-called pump field of the axion. The Fourier modes $\psi_{\mathbf{k}}(\eta)$ satisfy a canonical linear second-order equation, completely decoupled from the other fields,

$$\ddot{\psi}_{\mathbf{k}} + \left(k^2 - \frac{\ddot{a}_A}{a_A}\right)\psi_{\mathbf{k}} = 0. \tag{2.13}$$

This is the evolution equation for the axion field.

Equation (2.13) is equivalent to the equation for a classical harmonic oscillator with parametric evolution driven by the time dependent mass term $\ddot{a}_A/a_A$. When the time evolution of the velocity of the pump field, $\dot{a}_A$, is sufficiently slow such that, for a given mode k, $\ddot{a}_A/a_A \ll k^2$, we are in the adiabatic regime with the result that no particles are created. When the acceleration in the pump field is high enough to violate the adiabatic regime, quantum particle production starts. The evolution of the axion field and the resulting spectrum of particles are fully determined by the time behavior of the pump field in the different phases of the universe. In particular, a strong difference in this behavior exists between the pre-big bang phase and the standard radiation and matter dominated eras in the post-big bang universe.

The pre-big bang phase is characterized by an accelerated evolution of the pump field,

$$a_A \propto (-\eta)^\gamma, \quad \gamma = \frac{5\delta - 1}{2(1-\delta)}, \tag{2.14}$$

where $\delta < 0$ is the power which characterizes the evolution of the external dimensions, Eq. (2.9). Using Eq. (2.13), the evolution equation of the axion can be written as

$$\ddot{\psi}_{\mathbf{k}} + k^2\left(1 - \frac{\gamma(\gamma-1)}{x^2}\right)\psi_{\mathbf{k}} = 0, \tag{2.15}$$

where $x \equiv k\eta$. This equation is solved analytically in terms of the Hankel functions $\eta^{1/2}H_\mu^{(1)}$ and $\eta^{1/2}H_\mu^{(2)}$ with $\mu = |\gamma - 1/2|$.

At very early time, a perturbation of given wave number k is well inside the horizon, $|x| = |k\eta| \gg 1$, and the solutions of Eq. (2.15) are harmonic oscillations which can be consistently normalized to the vacuum fluctuation spectrum for $\eta \to -\infty$. This initial condition implies that the $H_\mu^{(1)}$ mode is absent and

$$\psi_{\mathbf{k}}(\eta) = (-\eta)^{1/2}H_\mu^{(2)}(k\eta), \quad \mu = \frac{1}{2} - \gamma = \frac{1-3\delta}{1-\delta},$$

$$\text{for} \quad \eta < -\eta_1. \tag{2.16}$$

Here $-\eta_1 \to \eta_1$ is the transition time scale between the pre-big bang phase and the standard radiation dominated era.

After the singularity, during the standard radiation and matter dominated eras, the dilaton is frozen, $\phi = \text{const}$, and the pump field is proportional to the standard scale factor, $a_A \propto a$. The scale factor, a, and its second derivative, $\ddot{a}$, are given by Friedman's equations. For a critical universe, which we consider throughout our calculations and which is certainly a good approximation until redshifts $z \lesssim 5$, we have

$$\frac{\ddot{a}}{a} = \frac{4\pi G}{3} a^2 (\rho - 3p) + \frac{2a^2 \Lambda}{3}, \qquad (2.17)$$

$$\frac{\dot{a}^2}{a^2} = \frac{8\pi G}{3} a^2 \rho + \frac{a^2 \Lambda}{3}. \qquad (2.18)$$

Energy conservation for radiation (r) and matter (m) yields $\rho_r \propto 1/a^4$ and $\rho_m \propto 1/a^3$, with $\rho = \rho_r + \rho_m$ and $p = \rho_r/3$; ρ_r is the radiation energy density, ρ_m is the matter energy density, and p the pressure of the radiation fluid. At early times, when Λ is negligible, these equations have a simple analytical solution,

$$a = a_{\text{eq}} (\eta / \eta_* + \tfrac{1}{4} (\eta / \eta_*)^2),$$

$$\eta_* \equiv \left(\frac{3}{4\pi G \rho_{\text{eq}}} \right)^{1/2} = \frac{\eta_{\text{eq}}}{2(\sqrt{2}-1)} \simeq 1.2 \, \eta_{\text{eq}}, \qquad (2.19)$$

where η_{eq} is the transition time between the radiation and the matter dominated era, $\rho_r(\eta_{\text{eq}}) = \rho_m(\eta_{\text{eq}}) = \rho_{\text{eq}}/2$. The mass term during the post-big bang becomes

$$\frac{\ddot{a}_A}{a_A} = \frac{\ddot{a}}{a} = \frac{1}{2\eta\eta_* + \tfrac{1}{2}\eta^2}. \qquad (2.20)$$

When Λ is nonvanishing, the solution for the effective potential can be found numerically but since the contribution of a small cosmological constant to the scale factor becomes important only at late time, the solutions to (2.15) are almost unaffected; this has been checked by numerical tests. In the radiation dominated era, $\eta < \eta_{\text{eq}}$, the mass term can be approximated by $\ddot{a}_A / a_A \simeq 1/(2\eta_* \eta)$.

We now study the axion evolution in the post-big bang era. Let us write the term in parentheses on the left-hand side of the axion equation of motion, Eq. (2.13), as

$$\left(k^2 - \frac{\ddot{a}}{a} \right) = k^2 \left(1 - \frac{(\ddot{a}/a)\eta^2}{x^2} \right) = k^2 \left(1 - \frac{\eta/(2\eta_* + \eta/2)}{x^2} \right). \qquad (2.21)$$

In order to study the solution of Eq. (2.13) we have to study the ratio of the dimensionless mass term $(\ddot{a}/a)\eta^2$ and x^2 to be compared with unity. As long as we are well in the radiation dominated era, $\eta \ll \eta_*$, the dimensionless mass term is small and particle creation induced by the pump field is negligible at early times. Equation (2.13) then is a harmonic equation solved by free plane waves,

$$\psi_{\mathbf{k}}(\eta) = \frac{1}{\sqrt{k}} [c_+(\mathbf{k}) e^{-ik\eta} + c_-(\mathbf{k}) e^{ik\eta}]. \qquad (2.22)$$

By matching the two solutions (2.16) and (2.22) at the transition time η_1 we obtain, for $|k\eta_1| \ll 1$ and $\eta_{\text{eq}} \gg \eta > \eta_1$,

$$c_\pm(\mathbf{k}) = \pm c(\mathbf{k}) \quad \text{with} \quad \langle |c(\mathbf{k})|^2 \rangle \simeq \begin{cases} \left(\dfrac{k}{k_1} \right)^{-2\mu - 1}, & k < k_1, \\ 0, & k > k_1, \end{cases}$$

$$(2.23)$$

so that

$$\psi_{\mathbf{k}} = \frac{c(\mathbf{k})}{\sqrt{k}} \sin(k(\eta - \eta_1)) \quad \text{for} \quad \eta_1 < \eta \ll \eta_{\text{eq}}. \quad (2.24)$$

Here $k_1 = 1/\eta_1$ represents the maximal amplified frequency of the pre-big bang phase. As already discussed in the introduction we suppose that modes with frequencies much lower than k_1 are unaffected by the unknown details of the transition from the pre- to the post-big bang phase.

The energy-density distribution of the produced axions is then

$$\frac{d\rho_\sigma(\mathbf{k})}{d\log k} \simeq \frac{1}{\pi^2} \left(\frac{k}{a} \right)^4 \langle |c(\mathbf{k})|^2 \rangle \simeq \left(\frac{k_1}{a} \right)^4 \left(\frac{k}{k_1} \right)^{3-2\mu} \propto k^{n_\sigma - 1}. \qquad (2.25)$$

The axion spectral index n_σ is related to the power which characterizes the evolution of the external dimensions by

$$n_\sigma = 4 - 2\mu = 3 + 2\gamma = 2 \left(\frac{1+\delta}{1-\delta} \right), \qquad (2.26)$$

which follows from Eq. (2.16). In order not to over-produce infrared axions we have to require $\mu \leq 3/2$, or $n_\sigma \geq 1$, which implies $\delta \geq -1/3$. As already pointed out in Ref. [22], the limiting value $\mu = 3/2$ corresponds precisely to a Harrison–Zel'dovich spectrum of CMB anisotropies on large scale. In terms of the evolution of the scale factor, this corresponds to an isotropic expansion and contraction, respectively, of the external and internal dimensions,

$$a \propto \frac{1}{e^\beta} \propto (-\eta)^{-1/3}. \qquad (2.27)$$

Notice that only for a 10-dimensional spacetime, symmetrical expansion and contraction corresponds to a flat axion spectrum which induces a Harrison–Zel'dovich spectrum of CMB fluctuations [23,22].

Nevertheless, as will be discussed in Sec. IV, at very large scales and very early (negative) times, we will need a slightly blue axion spectrum to fit CMB data. This requires a somewhat larger value of δ, i.e., a slower expansion of the external dimensions and, correspondingly, a somewhat faster contraction of internal dimensions at early time. This blue spectrum cannot be maintained up to the string scale because the fixed normalization at the string scale to $g_1^2 = [(k_1/a_1)/m_{\text{Planck}}]^2 \sim 0.01 - 10^{-4}$ would lead to much too small amplitudes at the COBE scale.

Let us therefore investigate what happens if the universe expands with some expansion law described by δ_- at early
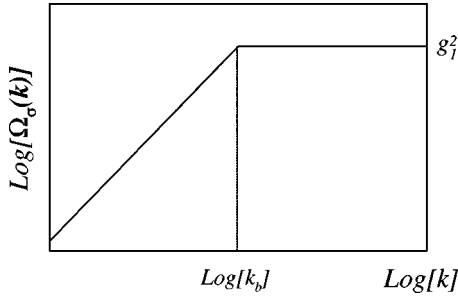
FIG. 1. Evolution of the axion spectral index during the pre-big bang. The value g_1 is the string coupling constant given by the string scale divided by the Planck scale, $g_1 = (k_1/a_1)/m_{\text{Planck}}$ (see Sec. IV).

times, $\eta < \eta_b < -\eta_1$ and then switches to an expansion law given by δ_+ after η_b. Sufficiently short wavelength modes which are inside the horizon during the entire epoch $\eta < \eta_b$, which satisfy $|k\eta_b| > 1$, are not influenced by this change in the expansion law. The term $\ddot{a}_A/a_A$ is indeed subdominant in the equation of motion for ψ_k during this epoch and hence the Bogoliubov coefficient $|c(\mathbf{k})|^2$ of Eq. (2.23) is not influenced by the transition; we just obtain the result (2.23) with $\mu = \mu_+$.

The situation is different if a mode exits the horizon before η_b. Then the "incoming" solution $\psi(\eta < \eta_b) = (-\eta)^{1/2} H^{(2)}_{\mu_-}(k\eta)$ differs from the vacuum solution and matching it to the general "outgoing" solution, $\psi(\eta > \eta_b) = b_1(-\eta)^{1/2} H^{(1)}_{\mu_+}(k\eta) + b_2(-\eta)^{1/2} H^{(2)}_{\mu_+}(k\eta)$, yields $b_2 - b_1 = (\Gamma(\mu_-)/\Gamma(\mu_+))|k\eta_b/2|^{\mu_+ - \mu_-}$. Correspondingly, the coefficient $|c(\mathbf{k})|^2$ is changed by a factor $|b_2 - b_1|^2$. In a model where the expansion law changes at a well defined time $\eta_b \equiv -1/k_b$, we therefore get the following Bogoliubov coefficients in the post-big bang radiation era (see Fig. 1):

$$\langle|c(\mathbf{k})|^2\rangle \simeq \left(\frac{k}{k_1}\right)^{-1-2\mu_+} \begin{cases} (k/k_b)^{2\mu_+ - 2\mu_-} & \text{for } k \lesssim k_b, \\ 1 & \text{for } k \gtrsim k_b. \end{cases}$$

$$(2.28)$$

We do not want to specify the event which may have triggered such a transition from $n_\sigma(k < k_b) = 4 - 2\mu_- = 1 + \varepsilon$ to $n_\sigma(k > k_b) = 1$, but there are certainly different possibilities. For example, it is interesting to note that isotropic expansion and contraction, $a \propto 1/b$, in a 26-dimensional space time gives $\delta_- = 1/5$, or $n_\sigma = 1.33$, which corresponds to $\varepsilon = 1/3$, just about the "tilt" needed to fit the observed CMB anisotropies (see Sec. III). Therefore, if we start out the pre-big bang phase with a 26-dimensional bosonic string vacuum (which we know to be unstable due to the presence of tachyons) which then "decays" to a supersymmetric and 10-dimensional string vacuum at some time η_b, which corresponds to a comoving energy scale k_b, this could induce the required tilt.

We now study the modification in the axion spectrum during the post-big bang era, where $a_A = a$. As we have seen above, during the radiation era, $\eta < \eta_*$, the dimensionless mass term is small. Furthermore, once a mode enters the horizon, $k\eta > 1$, the k^2 term always dominates over the mass
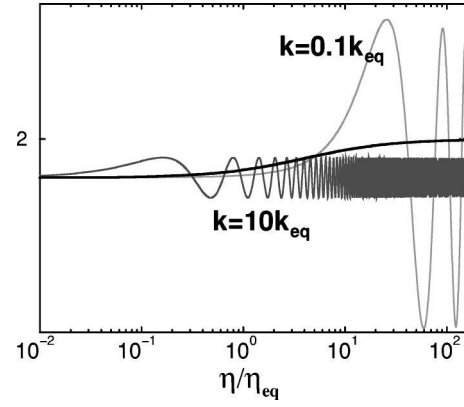

FIG. 2. The dimensionless effective mass $(\ddot{a}/a)\eta^2$ (thick line) and two modes that enter the horizon before and after equality. The mode that enters the horizon before equality, $\varphi(k = 10k_{\text{eq}}, \eta)$, is unaffected by the pump field and begins to oscillate without being amplified. The mode that enters the horizon after equality, $\varphi(k = 0.1k_{\text{eq}}, \eta)$, is amplified and begins to oscillate later.

term and there is no more particle creation. Therefore modes which enter the horizon before equality, $k\eta_* \gtrsim 1$, are not amplified any further in the post-big bang phase. The spectrum of axion perturbations for these modes remains unaffected. However, the low frequency tail of the spectrum is further modified as soon as we enter the matter dominated era, where the dimensionless mass term becomes of order unity. The modes which enter the horizon after equality, $k\eta_* \lesssim 1$, are amplified. This amplification of low frequency modes has important consequences on the angular spectrum of the CMB as we shall discuss in detail in Sec. III B.

The behavior of the dimensionless mass term $(\ddot{a}/a)\eta^2$ together with two modes that enter the horizon before and after equality have been plotted in Fig. 2. As one can see, only modes entering the horizon after equality are amplified. Deep in the matter era $\eta \gg \eta_{\text{eq}}$, the dimensionless mass term is constant and Eq. (2.13) becomes

$$\ddot{\psi}_k + \left(k^2 - \frac{2}{\eta^2}\right)\psi_k = 0.$$

$$(2.29)$$

This equation can again be solved in terms of Hankel functions,

$$\psi_k(\eta) = \eta^{1/2}[A H^{(2)}_{3/2}(k\eta) + B H^{(1)}_{3/2}(k\eta)] \quad \text{for } \eta \gg \eta_{\text{eq}},$$

$$(2.30)$$

where A and B are constants to be determined by matching conditions (see Ref. [23]). The post-big bang solutions (2.24) and (2.30) are only correct far from matter-radiation equality η_{eq} and in order to compute CMB anisotropies we require better precision for these solutions also for $\eta \sim \eta_{\text{eq}}$. We therefore solve the axion equation of motion Eq. (2.13) numerically, from the early radiation era through the radiation-matter transition.

The axion field is then given by

$$\sigma(\mathbf{k},\eta) = \frac{1}{a(\eta)}\psi_{\mathbf{k}}(\eta) = \frac{c(\mathbf{k})}{a\sqrt{k}}\varphi(k,\eta), \qquad (2.31)$$

where the variable φ is the solution of equation

$$\ddot{\varphi} + \left(k^2 - \frac{\ddot{a}}{a}\right)\varphi = 0 \qquad (2.32)$$

with initial condition [obtained from the pre-big bang solution Eq. (2.24)]

$$\varphi(k,\eta) = \sin(k\eta), \quad \eta \ll \eta_*. \qquad (2.33)$$

We have solved Eq. (2.32) numerically in this work using the effective potential (2.20). The prefactor $c(\mathbf{k})$ is a stochastic Gaussian field with power spectrum

$$\langle|c(\mathbf{k})|^2\rangle = (k/k_1)^{n_\sigma - 5}, \qquad (2.34)$$

where n_σ is again the primordial spectral index (2.26), our free parameter which depends on the higher-dimensional pre-big bang phase.

C. Axion quantum fluctuations as seeds

We are now ready to consider the axion field as a source of the linear cosmological perturbation equations. As in previous works [22–25] we suppose that the contribution of the axions to the cosmic fluid can be neglected and that they interact with it only gravitationally. They then play the role of seeds which, by their gravitational field, induce fluctuations in the cosmic fluid [21]. The back-reaction of the metric perturbations on the evolution of seeds is second order and can be neglected in first order perturbation theory. The evolution of axions can be computed by using the solutions of the axion field equation in the unperturbed background geometry, Eq. (2.13).

The axion field σ is a Gaussian stochastic variable. Its contribution to the perturbation equations is given in terms of its energy-momentum tensor,

$$T^{(\sigma)}_{\mu\nu} = \partial_\mu\sigma\partial_\nu\sigma - \tfrac{1}{2}g_{\mu\nu}(\partial_\alpha\sigma)^2, \qquad (2.35)$$

which is quadratic in σ and therefore not Gaussian. Moreover, although the axion field evolves according to a linear equation, it will enter into the perturbation equations through $T^{(\sigma)}_{\mu\nu}$ which evolves nonlinearly.

The perturbations in the dark matter and radiation components are set to zero in the initial conditions and are subsequently induced by the gravitational field of the axion. Hence, axion seed perturbations belong to the class of isocurvature perturbations. However, they differ from topological defects by being "acausal," i.e., they have nonvanishing correlations on super-Hubble scales, since they are due to field excitations induced during an inflationary era.

As we have seen above, the axion power spectrum obeys a simple power law with cutoff and is in general not analytic at $k=0$. Furthermore, axion perturbations do not, in general, display the scaling behavior expected from topological defects. In the pre-big bang we have an additional scale, the

string scale k_1, which breaks scale invariance. The axion spectrum on large scales is therefore not determined by dimensional arguments since there are dimensionless factors of the form $(k/k_1)^\alpha$ which may alter the spectrum.[1] The significance of these points will become clearer later in the paper.

As in Ref. [25], we first consider a critical universe (total density parameter $\Omega = 1$) consisting of cold dark matter, baryons, photons, and three types of massless neutrino, with or without a cosmological constant. We choose the baryonic density parameter $\Omega_b = 0.05$ and the value of the Hubble parameter $H_0 = 100h$ km s^{-1} Mpc^{-1} with $h = 0.65$.

The linear perturbation equations for this universe in Fourier space are of the form

$$\mathcal{D}X = S, \qquad (2.36)$$

where X is a long vector containing all the fluid perturbation variables which depends on the wave number $\mathbf{k}$ and conformal time η, S is a source vector which consists of certain combinations of the seed energy momentum tensor and $\mathcal{D}$ is a linear ordinary differential operator. More details on the linear system of differential equations (2.36) can be found in Ref. [32] and references therein.

For a given initial condition, this equation can in general be solved by means of a Green's function, $\mathcal{G}(\eta, \eta')$, in the form

$$X(\mathbf{k},\eta_0) = \int_{\eta_{in}}^{\eta_0} \mathcal{G}(\mathbf{k},\eta_0,\eta)\mathcal{S}(\mathbf{k},\eta)d\eta. \qquad (2.37)$$

We want to determine power spectra or, more generally, quadratic expectation values of the form

$$\langle X_i(\mathbf{k},\eta_0)X_j(\mathbf{k},\eta_0)^*\rangle, \qquad (2.38)$$

which, according to Eq. (2.37), are given by

$$\langle X_i(\mathbf{k},\eta_0)X_j(\mathbf{k},\eta_0)^*\rangle = \int_{\eta_{in}}^{\eta_0}\int_{\eta_{in}}^{\eta_0}\mathcal{G}_{il}(\eta_0,\eta)\mathcal{G}^*_{jm}(\eta_0,\eta')$$
$$\times\langle\mathcal{S}_l(\eta)\mathcal{S}^*_m(\eta')\rangle d\eta\, d\eta'. \quad (2.39)$$

(Sums over double indices are understood.)

We therefore have to compute the unequal time correlators $\langle\mathcal{S}_l(\eta)\mathcal{S}^*_m(\eta')\rangle$, of the seed energy-momentum tensor. This problem can, in general, be solved by an eigenvector expansion method [32,33], as it will be done in Sec. III B. However, if the source evolution is linear, the problem becomes especially simple. In this "coherent" case, we have

$$\mathcal{S}_j(\eta) = F_{ji}(\eta,\eta_{in})\mathcal{S}_i(\eta_{in}), \qquad (2.40)$$

---

[1] Actually the radiation-matter transition scale η_* represents a scale which is also present in models with topological defects, but deep in the radiation or matter era this scale has no significance, whereas as we shall see the above factors multiply the entire power spectrum of fluctuations.

with a deterministic transfer function F_{ji}. In this situation we can, by a simple change of variables, diagonalize the Hermitian, positive initial equal time correlation matrix,

$$\langle \mathcal{S}_l(\eta_{in})\mathcal{S}_m(\eta_{in})\rangle = \lambda_l \delta_{lm}.$$

Inserting this in Eq. (2.39) yields

$$\langle X_i(\eta)X_j^*(\eta')\rangle = \left(\int_{\eta_{in}}^{\eta_0}\mathcal{G}_{il}(\eta_0,\eta)F_{il}(\eta,\eta_{in})\sqrt{\lambda_l}\,d\eta\right)$$
$$\times\left(\int_{\eta_{in}}^{\eta_0}\mathcal{G}_{jm}(\eta_0,\eta')F_{jm}\right.$$
$$\left.\times(\eta',\eta_{in})\sqrt{\lambda_m}\,d\eta'\right)^*\delta_{lm}. \quad (2.41)$$

We therefore obtain exactly the same result as the one obtained by replacing the stochastic variable $\mathcal{S}$ by the deterministic source term $\mathcal{S}_j^{(det)}$ given by

$$\mathcal{S}_j^{(det)}(\eta)\mathcal{S}_i^{(det)}(\eta) = F_{jl}(\eta,\eta_{in})F_{il}(\eta,\eta_{in})\lambda_l$$
$$= \exp(i\theta_{ji})\sqrt{\langle|\mathcal{S}_j(\eta)|^2\rangle\langle|\mathcal{S}_i(\eta)|^2\rangle}, \quad (2.42)$$

where θ_{ji} is a, in principle unknown, phase which has to be determined case by case. Clearly $\theta_{jj}=0$. When the stochastic variable $\mathcal{S}$ is real (as in our case) $\exp(i\theta_{ji})=\pm1$. This linear or coherent approximation will be fully used in this paper. We shall test its validity in Sec. III B.

It is useful to split the energy-momentum tensor of the axion seeds (2.35) into a scalar, vector, and tensor part since the perturbations generated by each of these components evolves independently. Because of statistical isotropy these three modes are uncorrelated. This also corresponds to a decomposition of the source term $\mathcal{S}$ into a scalar, vector, and tensor contributions, $\mathcal{S}^{(S)}$, $\mathcal{S}^{(V)}$, and $\mathcal{S}^{(T)}$. A suitable parametrization of the decomposition of the Fourier components of $T_{\mu\nu}^{(\sigma)}$ is [21]

$$T_{00}^{(\sigma)} = f_\rho,$$

$$T_{j0}^{(\sigma)} = -ik_jf_v + v_j, \quad (2.43)$$

$$T_{ij}^{(\sigma)} = \delta_{ij}f_p - \left(k_ik_j - \frac{k^2}{3}\delta_{ij}\right)f_\pi + \frac{1}{2}(w_ik_j + w_jk_i) + \tau_{ij},$$

where f_ρ, f_v, f_p, and f_π are random function of $\mathbf{k}$; $\mathbf{w}$ and $\mathbf{v}$ are transverse vectors, $\mathbf{w}\cdot\mathbf{k}=\mathbf{v}\cdot\mathbf{k}=0$, and τ_{ij} is a symmetric, traceless, transverse tensor, $\tau_i^i=\tau_{ij}k^j=0$. The variables $(f_\bullet)$, $(\mathbf{v},\mathbf{w})$, and (τ_{ij}) represent the scalar, vector, and tensor degrees of freedom of $T_{\mu\nu}^{(\sigma)}$, respectively. They are the source of the perturbation equations.

The goal of the next three subsections is to express the correlators of the source components $\mathcal{S}^{(S)}$, $\mathcal{S}^{(V)}$, and $\mathcal{S}^{(T)}$ in terms of these variables. These expressions, inserted in the perturbation equation (2.36), then allow us to compute the CMB anisotropy and dark matter power spectra numerically.

D. Axion seeds—Scalar component

We first consider the scalar contribution given by the four variables $f_\bullet$ of Eq. (2.44). Only two of these functions are independent, the other two are related by energy and momentum conservation. We shall use two linear combinations of the three scalar seed functions f_ρ, f_v, and f_π:

$$f_\rho(\mathbf{k},\eta) = a^2\rho^{(\sigma)} = T_{00}^{(\sigma)}(\mathbf{k},\eta), \quad (2.44)$$

$$f_v(\mathbf{k},\eta) = \frac{ik^jT_{0j}^{(\sigma)}(\mathbf{k},\eta)}{k^2}, \quad (2.45)$$

$$f_\pi(\mathbf{k},\eta) = \frac{3}{2k^4}\left[-T_{ij}^{(\sigma)}(\mathbf{k},\eta)k^ik^j + \frac{1}{3}k^2\delta^{kl}T_{kl}^{(\sigma)}(\mathbf{k},\eta)\right]. \quad (2.46)$$

In the presence of seeds and in the linear perturbation approximation, the scalar component of the total geometric perturbations determined by the Bardeen potentials Φ and Ψ can be separated into a part induced by the seeds, Ψ_s and Φ_s, given by

$$k^2\Phi_s = 4\pi G[f_p + 3(\dot{a}/a)f_v)], \quad \Phi_s + \Psi_s = -8\pi Gf_\pi, \quad (2.47)$$

and a part induced by the perturbations of the cosmic fluid, Ψ_m and Φ_m. The total geometric perturbations are given by the sums,

$$\Psi = \Psi_s + \Psi_m, \quad \Phi = \Phi_s + \Phi_m. \quad (2.48)$$

The Bardeen potentials are gauge invariant and fully describe scalar perturbations of the Friedmann geometry (for details look in Refs. [34,35]).

Scalar perturbations are seeded by Φ_s and Ψ_s. These are the standard independent variables to use as scalar sources in the perturbation equations. In order to simplify somewhat the computation, we use Φ_s and f_π as our scalar seed degrees of freedom and the scalar source vector becomes

$$\mathcal{S}^{(S)}(\mathbf{k},\eta) = [\Phi_s(\mathbf{k},\eta), 4\pi Gf_\pi(\mathbf{k},\eta)]. \quad (2.49)$$

The energy-momentum tensor of the axion is given by Eq. (2.35), which leads to the following expressions for the seed functions in terms of the axion field σ:

$$f_\rho(\mathbf{k},\eta) = \frac{1}{2}\int\frac{d^3p}{(2\pi)^3}[\dot{\sigma}(\mathbf{p},\eta)\dot{\sigma}(|\mathbf{k}-\mathbf{p}|,\eta)$$
$$-\mathbf{p}\cdot(\mathbf{k}-\mathbf{p})\sigma(\mathbf{p},\eta)\sigma(|\mathbf{k}-\mathbf{p}|,\eta)], \quad (2.50)$$

$$f_v(\mathbf{k},\eta) = -\frac{1}{k^2}\int\frac{d^3p}{(2\pi)^3}\mathbf{k}\cdot(\mathbf{k}-\mathbf{p})\dot{\sigma}(\mathbf{p},\eta)\sigma(|\mathbf{k}-\mathbf{p}|,\eta), \quad (2.51)$$

$$f_\pi(\mathbf{k}, \eta) = -\frac{3}{2k^4} \int \frac{d^3p}{(2\pi)^3} \left[(\mathbf{k}\cdot\mathbf{p})[\mathbf{k}\cdot(\mathbf{k}-\mathbf{p})] \right.$$

$$\left. -\frac{1}{3}k^2\mathbf{p}\cdot(\mathbf{k}-\mathbf{p}) \right] \sigma(\mathbf{p}, \eta)\sigma(|\mathbf{k}-\mathbf{p}|, \eta).$$

$$(2.52)$$

The first two seed functions, f_ρ and f_v, together with Eq. (2.47), yield Φ_s,

$$\Phi_s(\mathbf{k}, \eta) = \frac{4\pi G}{k^2} \int \frac{d^3p}{(2\pi)^3} \left[\frac{1}{2}\dot{\sigma}(\mathbf{p}, \eta)\dot{\sigma}(|\mathbf{k}-\mathbf{p}|, \eta) \right.$$

$$-\frac{1}{2}\mathbf{p}\cdot(\mathbf{k}-\mathbf{p})\sigma(\mathbf{p}, \eta)\sigma(|\mathbf{k}-\mathbf{p}|, \eta)$$

$$\left. -3\frac{\dot{a}}{a}\frac{\mathbf{k}\cdot(\mathbf{k}-\mathbf{p})}{k^2}\dot{\sigma}(\mathbf{p}, \eta)\sigma(|\mathbf{k}-\mathbf{p}|, \eta) \right].$$

$$(2.53)$$

The only information about the source random variables which we really need are the unequal time correlators between the Fourier components of the independent variables Φ_s and f_π. These correlators can be written in terms of four real [since the correlators $\langle\sigma(\mathbf{k}, \eta)\sigma^*(\mathbf{k}', \eta')\rangle$ are real] scalar source correlation functions, F_{11}, F_{22}, F_{12}, and F_{21}, which completely characterize the scalar component of the source,

$$\langle\Phi_s(\mathbf{k}, \eta)\Phi_s^*(\mathbf{k}', \eta')\rangle = \delta(\mathbf{k}-\mathbf{k}')F_{11}(k, \eta, \eta'),$$

$$4\pi G\langle\Phi_s(\mathbf{k}, \eta)f_\pi^*(\mathbf{k}', \eta')\rangle = \delta(\mathbf{k}-\mathbf{k}')F_{12}(k, \eta, \eta'),$$

$$4\pi G\langle f_\pi(\mathbf{k}, \eta)\Phi_s^*(\mathbf{k}', \eta')\rangle = \delta(\mathbf{k}-\mathbf{k}')F_{21}(k, \eta, \eta'),$$

$$(4\pi G)^2\langle f_\pi(\mathbf{k}, \eta)f_\pi^*(\mathbf{k}', \eta')\rangle = \delta(\mathbf{k}-\mathbf{k}')F_{22}(k, \eta, \eta').$$

Note that $F_{11}(k, \eta, \eta)$ and $F_{22}(k, \eta, \eta)$ are positive by definition and, since the functions F_* are real, $F_{ij}(k, \eta, \eta') = F_{ji}(k, \eta', \eta)$. In order to compute these functions we make use of Eqs. (2.52) and (2.53) and we exploit the stochastic average conditions of the Gaussian variables σ and $\dot{\sigma}$ (Wick's theorem). We first introduce three real auxiliary variables Σ_1, Σ_2, and Σ_3, which depend on the power spectrum of the axion field, $\langle|c(\mathbf{k})|^2\rangle$, and on the solution φ of the evolution equation, Eq. (2.32),

$$\langle\sigma(\mathbf{k}, \eta)\sigma(\mathbf{k}', \eta')\rangle = (2\pi)^3\delta(\mathbf{k}-\mathbf{k}')\Sigma_1(k, \eta, \eta'),$$

$$\langle\dot{\sigma}(\mathbf{k}, \eta)\dot{\sigma}(\mathbf{k}', \eta')\rangle = (2\pi)^3\delta(\mathbf{k}-\mathbf{k}')\Sigma_2(k, \eta, \eta'),$$

$$\langle\sigma(\mathbf{k}, \eta)\dot{\sigma}(\mathbf{k}', \eta')\rangle = (2\pi)^3\delta(\mathbf{k}-\mathbf{k}')\Sigma_3(k, \eta, \eta'),$$

$$(2.54)$$

$$\langle\dot{\sigma}(\mathbf{k}, \eta)\sigma(\mathbf{k}', \eta')\rangle = (2\pi)^3\delta(\mathbf{k}-\mathbf{k}')\Sigma_3(k, \eta', \eta).$$

The variables Σ_i are given by

$$\Sigma_1(k, \eta, \eta') = \frac{\langle|c(\mathbf{k})|^2\rangle}{ka(\eta)a(\eta')}\varphi(k, \eta)\varphi(k, \eta'), \quad (2.55)$$

$$\Sigma_2(k, \eta, \eta') = \frac{\langle|c(\mathbf{k})|^2\rangle}{ka(\eta)a(\eta')}[\dot{\varphi}(k, \eta) - \mathcal{H}(\eta)\varphi(k, \eta)]$$

$$\times[\dot{\varphi}(k, \eta') - \mathcal{H}(\eta')\varphi(k, \eta')], \quad (2.56)$$

$$\Sigma_3(k, \eta, \eta') = \frac{\langle|c(\mathbf{k})|^2\rangle}{ka(\eta)a(\eta')}[\dot{\varphi}(k, \eta) - \mathcal{H}(\eta)]\varphi(k, \eta'),$$

$$(2.57)$$

where $\mathcal{H} \equiv \dot{a}/a$. Notice that $\Sigma_1(\eta, \eta)$ and $\Sigma_2(\eta, \eta)$ are positive by definition.

Inserting these results in Eqs. (2.52) and (2.53), and making use of Wick's theorem for the "random variable" $c(\mathbf{k})$, we can work out a somewhat lengthy but straightforward expression for the scalar source functions, F_{11}, F_{22}, F_{12}, and F_{21}, in terms of the variables Σ_1, Σ_2, and Σ_3:

$$F_{11}(k, \eta, \eta') = \frac{(4\pi G)^2}{k^4} \int \frac{d^3p}{(2\pi)^3} \left\{ \frac{1}{2}\Sigma_2(p, \eta, \eta')\Sigma_2(|\mathbf{k}-\mathbf{p}|, \eta, \eta') - \frac{1}{2}\mathbf{p}\cdot(\mathbf{k}-\mathbf{p})[\Sigma_3(p, \eta, \eta')\Sigma_3(|\mathbf{k}-\mathbf{p}|, \eta, \eta') \right.$$

$$+\Sigma_3(p, \eta', \eta)\Sigma_3(|\mathbf{k}-\mathbf{p}|, \eta', \eta)] - 3\frac{\mathbf{k}\cdot(\mathbf{k}-\mathbf{p})}{k^2}[\mathcal{H}(\eta)\Sigma_2(p, \eta, \eta')\Sigma_3(|\mathbf{k}-\mathbf{p}|, \eta, \eta')$$

$$+\mathcal{H}(\eta')\Sigma_2(p, \eta, \eta')\Sigma_3(|\mathbf{k}-\mathbf{p}|, \eta', \eta)] + \frac{1}{2}(\mathbf{p}\cdot(\mathbf{k}-\mathbf{p}))^2\Sigma_1(p, \eta, \eta')\Sigma_1(|\mathbf{k}-\mathbf{p}|, \eta, \eta')$$

$$+3\frac{(\mathbf{p}\cdot\mathbf{k}-p^2)(k^2-\mathbf{p}\cdot\mathbf{k})}{k^2}\times[\mathcal{H}(\eta)\Sigma_3(p, \eta', \eta)\Sigma_1(|\mathbf{k}-\mathbf{p}|, \eta, \eta') + \mathcal{H}(\eta')\Sigma_3(p, \eta, \eta')\Sigma_1(|\mathbf{k}-\mathbf{p}|, \eta', \eta)]$$

$$+9\frac{\mathcal{H}(\eta)\mathcal{H}(\eta')}{k^4}[(\mathbf{k}\cdot(\mathbf{k}-\mathbf{p}))^2\Sigma_2(p, \eta, \eta')\Sigma_1(|\mathbf{k}-\mathbf{p}|, \eta, \eta') + (\mathbf{k}\cdot(\mathbf{k}-\mathbf{p}))(\mathbf{k}\cdot\mathbf{p})\Sigma_3(p, \eta', \eta)$$

$$\left.\times\Sigma_3(|\mathbf{k}-\mathbf{p}|, \eta, \eta')] \right\},$$

$$F_{22}(k, \eta, \eta') = \frac{9(4\pi G)^2}{2k^8} \int \frac{d^3p}{(2\pi)^3} \left[(\mathbf{k}\cdot\mathbf{p})(\mathbf{k}\cdot(\mathbf{k}-\mathbf{p})) - \frac{1}{3}k^2\mathbf{p}\cdot(\mathbf{k}-\mathbf{p}) \right]^2 \Sigma_1(p, \eta, \eta')\Sigma_1(|\mathbf{k}-\mathbf{p}|, \eta, \eta'),$$

$$F_{12}(k,\eta,\eta') = -\frac{3(4\pi G)^2}{2k^6} \int \frac{d^3p}{(2\pi)^3} \left[(\mathbf{k}\cdot\mathbf{p})(\mathbf{k}\cdot(\mathbf{k}-\mathbf{p})) - \frac{1}{3}k^2\mathbf{p}\cdot(\mathbf{k}-\mathbf{p}) \right]$$

$$\times \left[\Sigma_3(p,\eta',\eta)\Sigma_3(|\mathbf{k}-\mathbf{p}|,\eta',\eta) - \mathbf{p}\cdot(\mathbf{k}-\mathbf{p})\Sigma_1(p,\eta,\eta')\Sigma_1(|\mathbf{k}-\mathbf{p}|,\eta,\eta') \right.$$

$$\left. - 6\mathcal{H}(\eta)\frac{\mathbf{k}\cdot(\mathbf{k}-\mathbf{p})}{k^2}\Sigma_3(p,\eta',\eta)\Sigma_1(|\mathbf{k}-\mathbf{p}|,\eta,\eta') \right],$$

$$F_{21}(k,\eta,\eta') = F_{12}(k,\eta',\eta).$$

The scalar source correlators of the perturbation equation (2.36) can be written as a two by two positive and Hermitian matrix,

$$\langle \mathcal{S}_i^{(S)}(\mathbf{k},\eta)\mathcal{S}_j^{(S)*}(\mathbf{k},\eta')\rangle = \begin{bmatrix} F_{11}(k,\eta,\eta') & F_{12}(k,\eta,\eta') \\ F_{21}(k,\eta,\eta') & F_{22}(k,\eta,\eta') \end{bmatrix}.$$

$$(2.58)$$

E. Axion seeds—Vector component

The vector contribution to the perturbation equations is seeded by the vector seed functions v_i, Eq. (2.44),

$$v_i(\mathbf{k},\eta) = P_i^j T_{0j}^{(\sigma)}(\mathbf{k},\eta),\qquad (2.59)$$

where P_i^j is the projector operator onto the space orthogonal to $\mathbf{k}$ defined by

$$P_{ij} = \delta_{ij} - \hat{k}_i\hat{k}_j, \quad \hat{k}_i = k_i/k.\qquad (2.60)$$

Again, the second vector seed function, $\mathbf{w}$, is given by $\mathbf{v}$ via momentum conservations. Defining the projection of the vector $\mathbf{p}$ onto the space orthogonal to $\mathbf{k}$ by $\mathbf{p}^\perp = P\mathbf{p}$, we obtain an expression for the vector seed functions in terms of the axion field,

$$v_j(\mathbf{k},\eta) = i\int \frac{d^3p}{(2\pi)^3} p_j^\perp \dot{\sigma}(\mathbf{p},\eta)\sigma(\mathbf{k}-\mathbf{p},\eta).\quad (2.61)$$

We again need the unequal time correlators between the Fourier components of the vector seed functions v_i. These correlators can be written in terms of a vector source correlation function G, which completely characterize the vector component of the source [32],

$$(4\pi G)^2\langle v_i(\mathbf{k},\eta)v_j(\mathbf{k},\eta')\rangle = (\delta_{ij}-\hat{k}_i\hat{k}_j)G(k,\eta,\eta').$$

$$(2.62)$$

Using Eq. (2.61) and Eq. (2.54) this function takes the form

$$G(k,\eta,\eta') = \frac{(4\pi G)^2}{2k^2} \int \frac{d^3p}{(2\pi)^3} (k^2p^2 - (\mathbf{k}\cdot\mathbf{p})^2)$$

$$\times [\Sigma_2(p,\eta,\eta')\Sigma_1(|\mathbf{k}-\mathbf{p}|,\eta,\eta')$$

$$+ \Sigma_3(p,\eta,\eta')\Sigma_3(|\mathbf{k}-\mathbf{p}|,\eta',\eta)].$$

$$(2.63)$$

The vector source correlators of the perturbation equation (2.36) then are

$$\langle \mathcal{S}_i^{(V)}(\mathbf{k},\eta)\mathcal{S}_j^{(V)}(\mathbf{k},\eta')\rangle = P_{ij}G(k,\eta,\eta').\qquad (2.64)$$

F. Axion seeds—Tensor component

The tensor contribution to the perturbation equations is seeded by the tensor seed functions τ_{ij}, Eq. (2.43),

$$\tau_{ij}(\mathbf{k},\eta) = (P_i^k P_j^n - \tfrac{1}{2} P_{ij}P^{kn})T_{kn}^{(\sigma)}(\mathbf{k},\eta).\qquad (2.65)$$

This leads to an expression for the tensor seed function in terms of the axion field,

$$\tau_{ij}(\mathbf{k},\eta) = -\int \frac{d^3p}{(2\pi)^3} [p_i^\perp p_j^\perp - (1/2)(\delta_{ij} - \hat{k}_i\hat{k}_j)$$

$$\times (p^\perp)^2]\sigma(\mathbf{p},\eta)\sigma(\mathbf{k}-\mathbf{p},\eta),\qquad (2.66)$$

which can be used to compute the unequal time correlators. These correlators can be written in terms of a tensor source correlation function, H, which completely characterizes the tensor component of the source [32],

$$(4\pi G)^2\langle \tau_{ij}(\mathbf{k},\eta)\tau_{lm}(\mathbf{k},\eta')\rangle$$

$$= [\delta_{il}\delta_{jm} + \delta_{im}\delta_{jl} - \delta_{ij}\delta_{lm} + k^{-2}(\delta_{ij}k_lk_m + \delta_{lm}k_ik_j$$

$$- \delta_{il}k_jk_m - \delta_{im}k_lk_j - \delta_{jl}k_ik_m - \delta_{jm}k_lk_i)$$

$$+ k^{-4}k_ik_jk_lk_m]H(k,\eta,\eta')$$

$$= (P_{il}P_{jm} + P_{jl}P_{im} - P_{ij}P_{lm})H(k,\eta,\eta').\qquad (2.67)$$

Using Eq. (2.66) and Eq. (2.54) this function takes the form

$$H(k,\eta,\eta') = \frac{(4\pi G)^2}{4k^4} \int \frac{d^3p}{(2\pi)^3} (k^2p^2$$

$$- (\mathbf{k}\cdot\mathbf{p})^2)^2\Sigma_1(p,\eta,\eta')\Sigma_1(|\mathbf{k}-\mathbf{p}|,\eta,\eta').$$

$$(2.68)$$

The tensor source correlators of the perturbation equation, Eq. (2.36), hence are

$$\langle \mathcal{S}_{ij}^{(T)}(\mathbf{k},\eta)\mathcal{S}_{lm}^{(T)}(\mathbf{k},\eta')\rangle$$

$$= (P_{il}P_{jm} + P_{jl}P_{im} - P_{ij}P_{lm})H(k,\eta,\eta').\qquad (2.69)$$

III. CMB ANISOTROPIES INDUCED BY AXION SEEDS

In this section we present the CMB power spectrum obtained in our scenario. We first describe the CMB angular power spectrum obtained in the coherent approximation and in Sec. III B we then show in detail that the coherent approximation is very good for axionic seeds, leading to errors of 5% or less.

A. CMB power spectrum—coherent approximation

A source is called coherent [36,37] if the unequal time correlation functions can be factorized or replaced by the product of deterministic sources, as in Eq. (2.42),

$$\langle \mathcal{S}_j(\eta) \mathcal{S}_i(\eta') \rangle \simeq \pm \sqrt{\langle |\mathcal{S}_j(\eta)|^2 \rangle \langle |\mathcal{S}_i(\eta')|^2 \rangle}. \quad (3.1)$$

As pointed out in Sec. II C, this approximation is exact only if the source evolution is linear. Then the different **k** modes do not mix and the value of the source term at a fixed **k** at a later time is given by its value at initial time multiplied by some transfer function, as in Eq. (2.40). In this situation Eq. (3.1) becomes an equality and the model is perfectly coherent. This is not the case for our model since we know that, although the axion field evolves according to a linear equation, its energy-momentum tensor, which enters into the perturbation equations as source, does not; it is quadratic in the field σ. Thus, nonlinearity leads to mixing of scales and to deviation from a Gaussian distribution.

Nevertheless our situation is very similar to the large N limit of global $O(N)$ models in which the only nonlinearities also are the quadratic expressions of the energy-momentum tensor. In this case the effects of decoherence are very small and one finds that the full incoherent result is not very different from the perfectly coherent approximation [32].

This result motivated us to compute the CMB anisotropy in the perfectly coherent approximation. Here we repeat and expand on results already presented in Ref. [25] while in the next section we justify them by discussing the full incoherent case.

In order to compute the CMB anisotropy power spectrum in the coherent approximation, we replace the unequal time correlation functions in Eq. (2.39) by the products

$$\langle \mathcal{S}_i^{(S)}(\mathbf{k}, \eta) \mathcal{S}_j^{(S)}(\mathbf{k}, \eta') \rangle$$
$$= F_{ij}^{(n_\sigma)}(k, \eta, \eta')$$
$$\simeq \pm [F_{ij}^{(n_\sigma)}(k, \eta, \eta) F_{ij}^{(n_\sigma)}(k, \eta', \eta')]^{1/2},$$

$$\langle \mathcal{S}^{(V)}(\mathbf{k}, \eta) \mathcal{S}^{(V)}(\mathbf{k}, \eta') \rangle$$
$$= G^{(n_\sigma)}(k, \eta, \eta')$$
$$\simeq [G^{(n_\sigma)}(k, \eta, \eta) G^{(n_\sigma)}(k, \eta', \eta')]^{1/2}, \quad (3.2)$$

$$\langle \mathcal{S}^{(T)}(\mathbf{k}, \eta) \mathcal{S}^{(T)}(\mathbf{k}, \eta') \rangle = H^{(n_\sigma)}(k, \eta, \eta')$$
$$\simeq [H^{(n_\sigma)}(k, \eta, \eta) H^{(n_\sigma)}(k, \eta', \eta')]^{1/2},$$

where we have indicated the dependence of the correlators on the spectral index n_σ by a superscript. In Fig. 3 we show
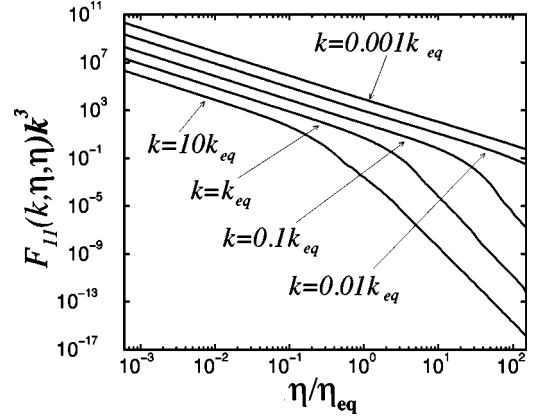

FIG. 3. Time evolution of the source function $F_{11}(k, \eta, \eta) k^3$, with tilt $n_\sigma = 1.1$, for different modes, $k = 0.001 k_{eq}$, $k = 0.01 k_{eq}$, $k = 0.1 k_{eq}$, $k = k_{eq}$, and $k = 10 k_{eq}$. For super-horizon modes, the correlator F_{11} decays like η^{1-2n_σ}/k^4. As soon as a mode enters the horizon the corresponding correlator decays faster due to the oscillating behavior of the axion field. Before crossing the horizon, the other scalar equal time correlators show the same power law behavior while the vector correlator $G(k, \eta, \eta) \propto \eta^{1-2n_\sigma}/k^2$ and the tensor correlator $H(k, \eta, \eta) \propto \eta^{1-2n_\sigma}$ (independent of k).

the time behavior of one of the equal time correlators. On super-horizon scales, $k\eta \ll 1$, they all display the same typical behavior, $\propto k^{-\kappa} \eta^{1-2n_\sigma}$, which depends on the spectral index n_σ and on κ, a positive power determined by dimensional arguments. On subhorizon scales the correlators decay fast due to incoherent oscillations of the convolved axion field.

We have solved Eq. (2.36) for the scalar, vector, and tensor components. The CMB anisotropy power spectrum is given by the sum of the three contributions and depends on the spectral index n_σ,

$$C_l^{(n_\sigma)} = C_l^{(Sn_\sigma)} + C_l^{(Vn_\sigma)} + C_l^{(Tn_\sigma)}. \quad (3.3)$$

In Fig. 4 we show the scalar, vector, and tensor contributions to the resulting CMB anisotropies for an axion spectrum with tilt $n_\sigma = 1.1$. The ''hump'' at $l \sim 60$ in the scalar component is due to the isocurvature nature of the perturbations. This is also one of the reasons why the acoustic peaks are very low, the other being that the vector (and tensor) component is of the same order of magnitude as the scalar one. This enhances, in seed models, the CMB spectrum at large scales thereby lowering the acoustic peaks at small scales. The result obtained is remarkably similar to the large N case studied in Ref. [32]. The main difference here is that, like for usual inflationary models, we dispose of a spectral index which is basically free. By choosing slightly bluer spectra, we can enhance the power on smaller scales.

In Fig. 5 we show the sum of the scalar, vector, and tensor contributions comparing the results from different tilts with and without a cosmological constant. The CMB power spectra obtained can have considerable acoustic peaks at $l \sim 250$ to 300, which can be raised further by adding a nonvanishing cosmological constant. Increasing the tilt n_σ raises the acoustic peaks and moves them to slightly smaller scales. As found in Ref. [23], the power spectrum of the scalar compo-
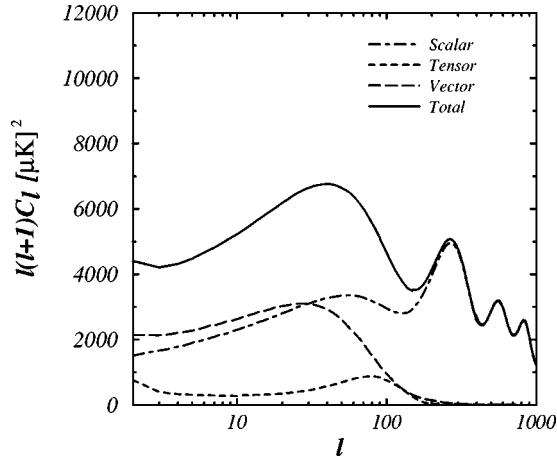
FIG. 4. The CMB anisotropy power spectrum for fluctuations induced by axion seeds with a tilt $n_\sigma = 1.1$ and $\Lambda = 0$. This result is computed within the coherent approximation. We show the scalar (dotted–dashed), vector (dashed), and tensor (dotted) contributions separately as well as their sum (solid).

nent is always blue. The tensor and vector component counterbalance the increase of the tilt, maintaining a nearly scale invariant spectrum on large scales. The models can be clearly discriminated from the common inflationary spectra by their isocurvature hump and by the position of the first peak. A discussion on the comparison of these results with recent CMB data will be given in Sec. IV.

We have also computed the CMB polarization for our model. The result for two different spectral indices is shown in Fig. 6 where we compare it with the polarization from usual inflationary models. It is interesting to note that our models show a characteristic ''polarization hump'' which is significantly smaller in inflationary models. The polarization ''hump'' is completely suppressed for topological defects due to causality [38] and represents a very characteristic signature of ''acausal seed models'' like the one under consideration.

B. Decoherence

In order to estimate the accuracy of the results found in the preceding subsection, we discuss here the decoherence of the axion seeds showing that the difference between the coherent approximation and the full incoherent calculation is very small. The decoherence is tested only for the scalar component of the spectrum, where it may lead to ''smearing out'' of the acoustic oscillations. Its effects on vector and tensor perturbations are expected to be small.

We first introduce the property of ''scaling'' for the axion seeds. When working with seeds, to solve the problem of the enormous dynamical range[2] needed to compute the C_l's

_____

[2]To compute the CMB and dark matter power spectra, we need to know the seed functions over a dynamical range of k_{max}/k_{min} $\sim 30\,000$ and this for all times $\eta_{in} \lesssim \eta$, $\eta' \leqslant \eta_0$ with $k\eta_{in} \ll 1$. This gives finally more than 1000 functions of two variables which have to be known accurately over a long time interval.
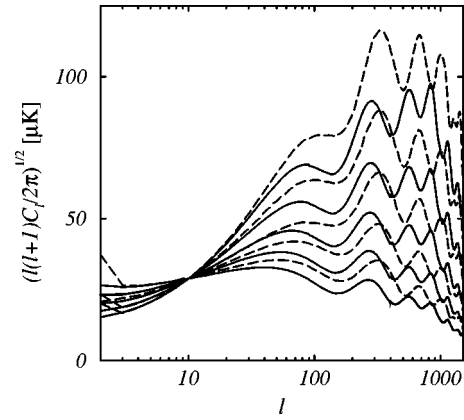

FIG. 5. The CMB anisotropy power spectrum for fluctuations induced by axion seeds. We show the sum of the scalar, vector, and tensor contributions for five different tilts, with $\Omega_\Lambda = 0$ (solid) and $\Omega_\Lambda = 0.7$ (long dashed). The tilt is raising from bottom to top, $n_\sigma = 1.1, 1.2, 1.3, 1.4, 1.5$.

from $l = 2$ to $l = 1500$, one often makes use of scaling properties. We call seeds scaling if their correlation function, $\langle \mathcal{S}(\mathbf{k}, \eta)\mathcal{S}(\mathbf{k}, \eta') \rangle$, is scale free, i.e., the only dimensional parameters in F_{ij}, G, and H are the variables η, η', and $\mathbf{k}$ themselves. As we have already mentioned, axion seeds are not scaling since the correlation function contains factors of the form $(k/k_1)^\alpha$. But such a simple prefactor can be written as

$$(k/k_1)^\alpha = (k\eta)^\alpha / (k_1\eta)^\alpha$$

and does not enter the costly numerical integration. Numerical calculations are reduced greatly if one can write the correlation function in the form

$$F_{ij}(\mathbf{k}, \eta, \eta') = f(\sqrt{\eta\eta'}, k_1) C_{ij}(y, r),$$

$$G(\mathbf{k}, \eta, \eta') = g(\sqrt{\eta\eta'}, k_1) W(y, r), \qquad (3.4)$$

$$H(\mathbf{k}, \eta, \eta') = h(\sqrt{\eta\eta'}, k_1) T(y, r),$$

where $y \equiv k\sqrt{\eta\eta'}$ and $r \equiv \sqrt{\eta'/\eta}$, and f, g, and h are given explicitly. The matrix C_{ij} and the functions W and T are dimensionless by construction. In the following we shall call this behavior ''modified scaling.''

But even after this extraction of the explicit breaking of scaling, our source does not exactly obey ''modified scaling'' due to the radiation-matter transition. As one can see immediately from the evolution equation of the axions in the post-big bang phase, Eq. (2.32), the extra dimensional parameter implicitly contained in the unequal time correlators is η_* which comes from the expression for the scale factor a, Eq. (2.19). The radiation-matter transition introduces the new scale η_* and thereby spoils the modified scaling behavior of the axion seeds.[3] However, deep in the radiation or

_____

[3]This breaking of scale invariance is also found in models with topological defects.
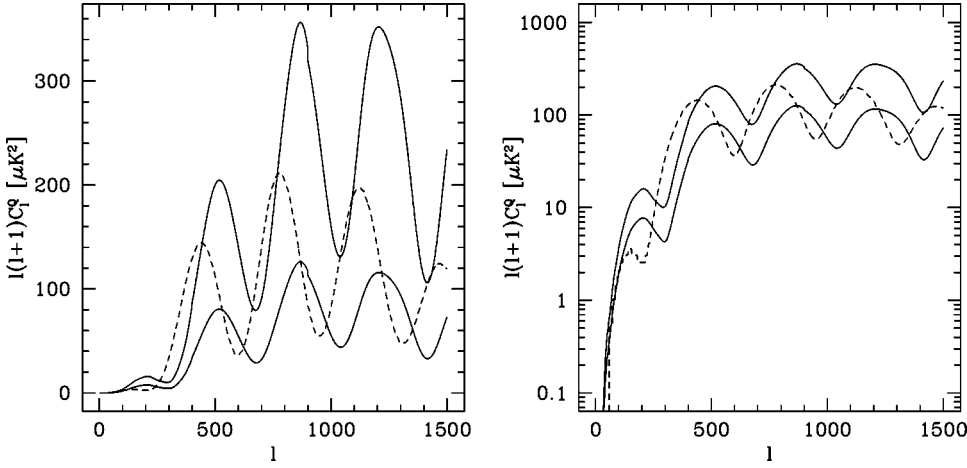
FIG. 6. The CMB polarization power spectrum in linear scale (left) and log scale (right) for fluctuations induced by axion seeds and shown for two different tilts, with $\Omega_\Lambda=0.7$, $n_\sigma=1.3$ (lower solid line), and $n_\sigma=1.5$ (upper solid line), are compared with the standard inflation result (dashed line) for the same cosmological parameters. Polarization clearly distinguishes between inflation and axion seeds, especially via the isocurvature hump.

matter era, $\eta \ll \eta_*$ or $\eta \gg \eta_*$, respectively, the reduced correlation functions do obey scaling. In order to avoid this problem and to simplify the numerical calculations, we therefore compute the axion field according to the equation for the pure radiation era, i.e., setting $a(\eta)=\eta$. We call this the radiation approximation. This approximation affects the correlators and the CMB anisotropy power spectrum, especially at large angular scales, but is expected not to differ significantly from the correct results on the scales of the acoustic peaks, and it allows us to obtain sources which obey modified scaling.

In the coherent case, where we just need the equal time correlators, the numerical requirements have not been very involved and we have not been pushed to the radiation approximation. But, as we shall see, the fully decoherent calculation will not change the results considerably and therefore an enormous numerical effort, which would be needed to compute the unequal time correlators without any use of scaling behavior, is not justified for this simple test.

In the matter dominated era, axion seeds are amplified by quantum particle creation while in the radiation approximation they do not experience this amplification. Nevertheless, axions are massless particles and they behave like a perfect radiation fluid. Thus, their energy density decreases as $1/a^4$, faster than the cosmic fluid in a matter dominated universe, where $a \propto \eta^2$ and $\rho \propto a^{-3}$, than in a radiation dominated universe, where $a \propto \eta$ and $\rho \propto a^{-4}$. This leads one to some overestimation of the sources at $\eta > \eta_*$ in the radiation approximation.

In Fig. 7 we compare the time behavior of one of the equal time correlators taking into account the radiation matter transition (dashed) with those obtained in the radiation approximation (solid line) for two different values of k. Modes that enter the horizon before matter-radiation equality, $k > k_{eq}$, do not feel quantum particle creation; therefore, there is no difference between the full result and the radiation approximation on super-horizon scales. Inside the horizon, in the matter era the mode decays faster than in the radiation approximation. Modes which enter the horizon after equality, $k < k_{eq}$, get first amplified by particle creation, an effect which is missed in the radiation approximation, but then decay faster than in the radiation approximation. As can be seen in Fig. 8, the slower decay has consequences on the

CMB anisotropy power spectrum: using the radiation approximation somewhat enhances the Sachs–Wolfe plateau and the first peak.

We now compute the CMB anisotropies in the full decoherent case for the radiation approximation, making use of modified scaling. We restrict our attention to the scalar component, where decoherence can be important.

As explained in Eq. (3.4) we write the scalar correlation matrix F_{ij} (for $n_\sigma=1$) as

$$F_{ij}(\mathbf{k},\eta,\eta')=(\eta\eta')^{3/2}C_{ij}(y,r), \qquad (3.5)$$

where C_{ij} is only function of y and r and hence dimensionless. The matrix C_{ij} is clearly symmetric under $r \to 1/r$ as
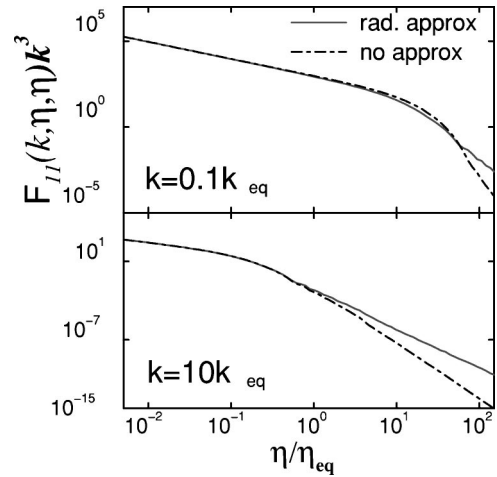

FIG. 7. Time behavior of $F_{11}(k,\eta,\eta)k^3$, with spectral index $n_\sigma=1.1$, for a mode which enters the horizon before matter-radiation equality, $\varphi(k=10k_{eq},\eta)$, and after, $\varphi(k=0.1k_{eq},\eta)$. Solid lines show the modes in the radiation approximation, dashed lines without approximation. For $k > k_{eq}$ there is no difference on super-horizon scales, while for $k < k_{eq}$ the additional amplification experienced in the matter dominated phase is lost in the radiation approximation. On subhorizon scales, the radiation approximation decays slower than the correct result. A similar behavior is found for the other correlators.
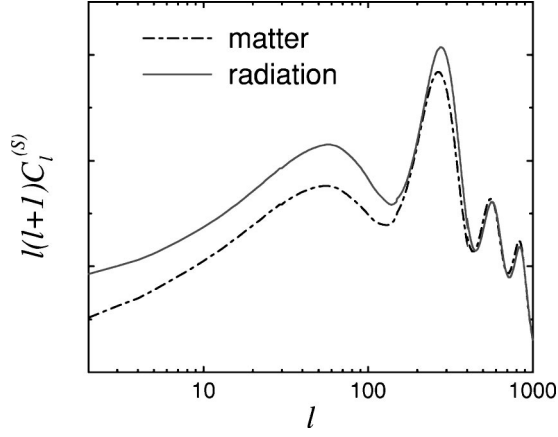
FIG. 8. Scalar contribution to the CMB angular power spectrum, computed in the pure radiation approximation (solid line) and without approximation (dashed line), with an axion spectral index $n_\sigma = 1.1$ and $\Lambda = 0$.
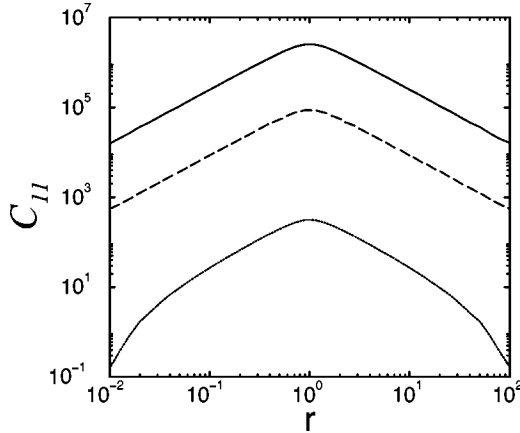
can be seen in Fig. 9. For $y < 1$ the sources decay like $1/y$ and after horizon crossing they begin to decay faster due to oscillations.

The source correlation matrix C_{ij} can now be considered as kernel of a positive Hermitian operator in the variables $x = k\eta = y/r$ and $x' = k\eta' = yr$, which can be diagonalized [32],

$$C_{ij}(x,x') = \sum_n \lambda_n v_{in}(x) v_{jn}(x'), \qquad (3.6)$$

where $\{v_{in}\}$ is an orthonormal series of eigenvectors (ordered according to the amplitude of the corresponding eigenvalues) of the operator C_{ij} for a given weight function w. The eigenvectors and the eigenvalues depend on the weight function w which can be chosen to optimize the speed of convergence of the sums (3.6).

Inserting Eq. (3.6) in Eq. (2.39) leads to

$$\langle X_i(\mathbf{k},\eta_0) X_j(\mathbf{k},\eta_0) \rangle = \sum_n \lambda^{(n)} X_i^{(n)}(\mathbf{k},\eta_0) X_j^{(n)}(\mathbf{k},\eta_0), \qquad (3.7)$$

where $X_i^{(n)}(\eta_0)$ is the solution of Eq. (2.36) with deterministic source term $v_i^{(n)}$,

$$X_j^{(n)}(\mathbf{k},\eta_0) = \int_{\eta_{in}}^{\eta_0} d\eta\, \mathcal{G}(\mathbf{k},\eta_0,\eta)_{jl} v_l^{(n)}(\mathbf{k},x). \qquad (3.8)$$

For the scalar CMB anisotropy spectrum this gives

$$C_l^{(S)} = \sum_{n=1}^N \lambda_n^{(S)} C_l^{(Sn)}; \qquad (3.9)$$

$C_l^{(S)}$ is the scalar component of the CMB anisotropy induced by the deterministic source v_n and N is the number of eigenvalues which have to be considered to achieve good accuracy.

In our model we actually find it easier to diagonalize the matrix

$$\tilde{C}_{ij}(x,x') = C_{ij}(x,x')\sqrt{xx'},$$

whose diagonal is flat for $x < 0.01$, exactly as in the large-N and texture models studied in Ref. [32]. In this case we have

$$C_{ij}(x,x') = \sum_n \tilde{\lambda}_n \frac{\tilde{v}_{in}(x)}{\sqrt{x}} \frac{\tilde{v}_{jn}(x')}{\sqrt{x'}}, \qquad (3.10)$$

where $\tilde{v}_{jn}$ and $\tilde{\lambda}_n$ are the eigenvectors and the eigenvalues of the matrix $\tilde{C}_{ij}$.

We diagonalize the matrix $\tilde{C}_{ij}$ using the logarithmic weight function $w = 1/x$ which allows us to sample the range of scales of interest more evenly. In Fig. 10 we show the eigenvectors decomposition of one of the scalar correlators. Note that a rather high number of eigenvectors and eigenvalues is required to reach a good accuracy in the approximation of the diagonal of the correlation function. Summing up
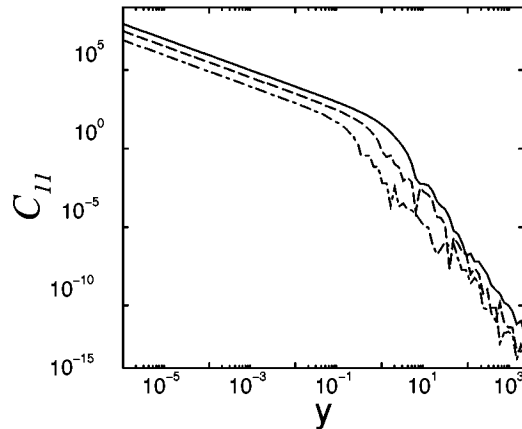

FIG. 9. The correlator $C_{11}(y,r)$ is shown. In the left panel the solid, dashed, and dotted lines, respectively, represent $C_{11}(1 \times 10^{-7}, r)$, $C_{11}(1 \times 10^{-4}, r)$, and $C_{11}(0.03, r)$. In the right panel the solid, dashed, and dotted lines, respectively, represent $C_{11}(y,1)$, $C_{11}(y,0.3)$, and $C_{11}(y,0.1)$. The other scalar correlators C_{22} and C_{12} behave similarly.
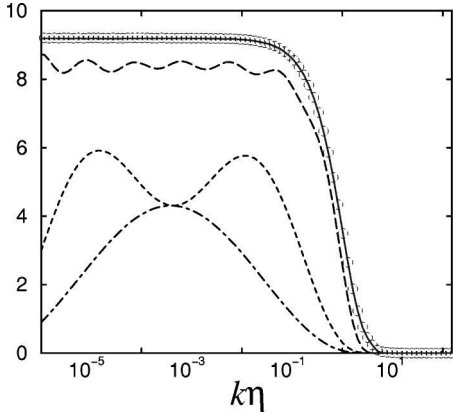
FIG. 10. The sum of the first few eigenfunctions of $\tilde{C}_{11}(x,x')$ is shown for a weight function $w = 1/x$. The first (dotted–dashed), first and second (short dashed), first 10 (long dashed), and 50 (solid) eigenfunctions are summed up. The open circles represent the full correlation function. Here we only show the equal time diagonal of the correlation matrix but the same convergence behavior is found in the C_l power spectrum which is sensitive to the full correlation matrix.

$N = 50$ eigenvectors the convergence is guaranteed; the summed up correlation function reproduces the original to better than 1%.

This is different from the large-N model, where about 20 eigenvectors suffice for the same accuracy. We assume that this difference is due to the slower decay of the source functions. As can be seen from Fig. 10, the source function is decaying from its original value to about 1% over the interval $0.1 < k\eta < 10$, while in the large-N model this decay is achieved in the interval $0.5 < k\eta < 4$.

We now compute the scalar contribution to the CMB anisotropies using Eq. (3.9). The result is shown in Fig. 11. We note that decoherence slightly reduces the amplitude of
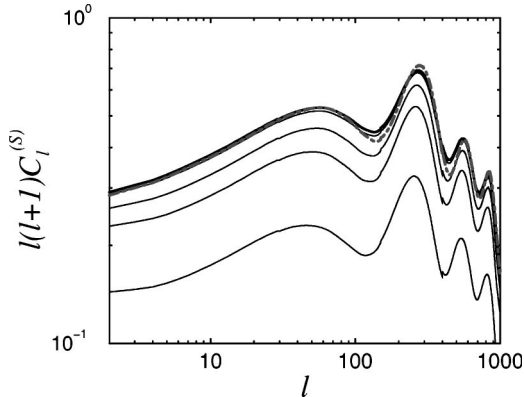

FIG. 11. The scalar contribution to the $C_l^{(S)}$ power spectrum is shown for a primordial spectral index $n_\sigma = 1.1$. From bottom to top, the solid lines show the contributions of the sum of the first ten, first twenty, first thirty and first forty $C_l^{(Sn)}$'s. The thick solid line represents the full eigenvectors summation (up to $N = 50$) to be compared to the perfect coherent approximation, shown by the dashed line. The decoherence does not significantly wash out the acoustic peak and the oscillations.

the oscillations around the first peak leaving however the secondary peaks and their positions almost unaffected. Although axion perturbations are in principle incoherent, it is difficult to observe this from the CMB power spectrum. The effects of decoherence are indeed very weak and the spectrum obtained in the perfect coherent approximation reproduces the decoherent result within less than 5%. We hence are confident to obtain a sufficient accuracy in the perfectly coherent approximation which we shall apply for the rest of this paper.

IV. COMPARISON WITH CMB ANISOTROPY DATA AND MATTER PERTURBATIONS

In this section we compare the results found in the preceding section with data discussing in particular the consequences of the normalization of CMB anisotropies to COBE and presenting the cosmological parameters favored by our model. In Sec. IV D we finally compute the dark matter power spectrum and we compare it with data.

A. Normalization and the kink

Comparing our numerical result with the CMB data we normalize our curve to the fluctuation amplitude observed by COBE. This provides a relation between the string scale and the scale of the break k_b. Since we ignore constant factors of order unity in the overall amplitude in our calculation, the result for the amplitude is not very precise, but certainly correct within a factor of about 2. For the best fit value of the tilt, $n_\sigma - 1 = \varepsilon \sim 0.33$, our numerical result on the COBE scale (at $l \sim 10$) is $l(l+1)C_l \simeq 0.3 g_1^4 (\eta_* k_b)^{-2\varepsilon}$. Here g_1 is the dimensionless string coupling constant given by $\omega_1 / m_{\text{Planck}}$ where $\omega_1 = k_1 / a_1 = H(\eta_1)$ is the inverse string scale. Comparing this with the COBE normalization, $l(l+1)C_l T_0^2 \simeq 5225 \, \mu\text{K}^2$, yields

$$\eta_* k_b = (2.1 \times 10^3 g_1^2)^{1/\varepsilon}. \tag{4.1}$$

For example, if the string scale is 10^{18} GeV, so that $g_1 \sim 0.1$, we get $k_b \sim h^2 / (2 \text{ kpc})$, where we have inserted $\eta_* \sim 20 h^2$ Mpc. An interesting constraint comes from the fact that the break in the spectrum should be on a scale which is smaller than the scale represented by the first acoustic peak in order not to reduce the latter. Since η_* corresponds to the horizon scale at equality, this requires $\eta_* k_b \gtrsim 1$ or $\omega_1(a_1) = H_1 \gtrsim 0.02 m_{\text{Planck}}$. Together with $H_1 \lesssim 0.1 m_{\text{Planck}}$, this brackets the string scale just in the range where it is expected for very different theoretical reasons.

The length-scale/energy-scale corresponding to the break k_b at the time η_b, during the pre-big bang phase, when the expansion law is supposed to change, is given by

$$|t_b| \sim |\eta_b| a(\eta_b) / a_0$$

$$\sim |\eta_b| \frac{a(\eta_b)}{a(\eta_1)} 10^{-32}$$

$$\sim |\eta_b| \left| \frac{\eta_b}{\eta_1} \right|^{-1/4} 10^{-32} \sim 6 \times 10^{-14} \text{ cm} \sim 3 \text{ GeV}^{-1},$$
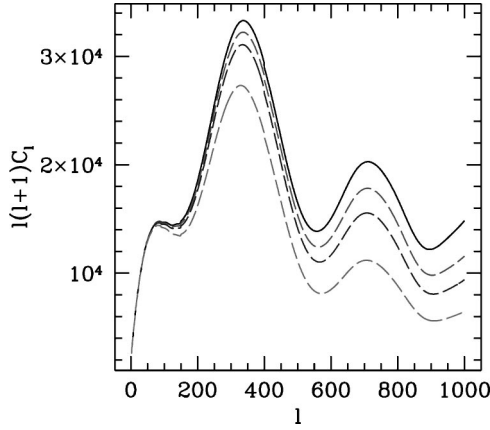
$$\tag{4.2}$$

FIG. 12. The influence of the break position on the CMB power spectrum. The top solid line is the spectrum without break. The dashed lines from top to bottom represent a spectrum with break at $k_b = 3/\eta_*$, $2/\eta_*$, and $1/\eta_*$, respectively.

where we have used $\eta_b \sim \eta_* \sim 20$ Mpc and $\eta_1 \sim 0.1$ cm. The energy scale obtained in this way is uncertain with a factor of about 10.

In Fig. 12 we show the dependence of the CMB anisotropy spectrum on the position of the break. Typically, the break lowers the second and subsequent acoustic peaks while it does not substantially affect the first peak.

B. Cosmological parameters

In the last two years, a peak in the CMB power spectrum at $l \sim 200$ as been detected by several different experiments, most notably TOCO98 [1], B97 [2], B98 [3], and MAXIMA-1 [4]. Among them, the BOOMERanG-98 power spectrum [3] reported the best and at the same time most conservative detection, although coming from only 5% of their overall data set. The position, amplitude and shape of the peak can be fitted by the power spectra expected in the simplest inflationary scenario based on adiabatic perturbations in a spatially flat universe [5,8]. Therefore, this peak represents the biggest challenge for the model presented here.

We want to investigate whether a suitable choice of cosmological parameters can bring our model in agreement with the above mentioned data. This question is also very important in view of the usual ''determination of the cosmological parameters'' from CMB anisotropies, in the sense that it shows how the results can change when assuming a different model of structure formation. In other words the so-called ''measurements'' of cosmological parameters from CMB anisotropies are strongly model dependent.

The peak position is determined mainly by the angular diameter distance parameter

$$R^{-1} = \sqrt{\frac{\Omega_m}{|\Omega_K|}} \frac{F(y)}{2}. \tag{4.3}$$

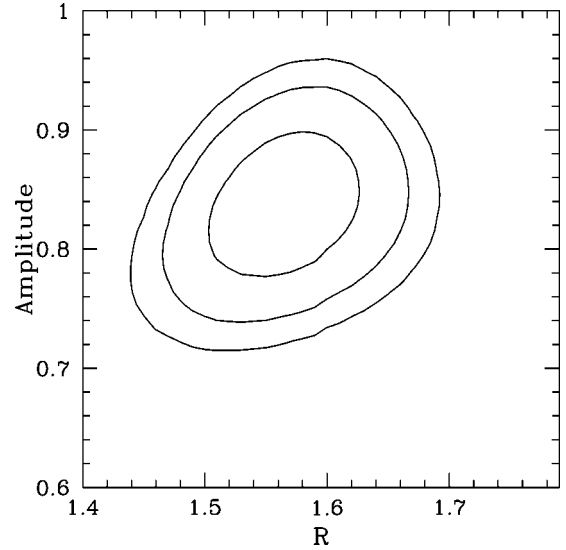Here $\Omega_K = 1 - \Omega_m - \Omega_\Lambda$ is the curvature parameter and

FIG. 13. Confidence levels (68%, 95%, and 99%) for the rescaling factor R and the amplitude in COBE units A, from the recent BOOMERanG and MAXIMA-1 observations.

$$F(y) = \begin{cases} \sinh y & \text{(open)} \\ y & \text{(flat)} \\ \sin y & \text{(closed)} \end{cases} \tag{4.4}$$

depends on the geometry of the universe. The variable y is the following integral:

$$y = \sqrt{|\Omega_K|} \int_0^{z_{\text{dec}}} \frac{dz}{[\Omega_m(1+z)^3 + \Omega_K(1+z)^2 + \Omega_\Lambda]^{1/2}}. \tag{4.5}$$

As pointed out in Ref. [39], the condition $R = $ constant identifies curves in the $\Omega_m - \Omega_\Lambda$ plane, with nearly degenerate C_l spectra, providing that the baryon density parameter Ω_{baryon} is kept constant.

In Fig. 13 we plot likelihood contours, obtained as follows: we rescale the string cosmology power spectra plotted in Fig. 5, both in amplitude A (in COBE units) and position R. We compare the resulting spectra with the BOOMERanG and MAXIMA-1 data in the region up to $l \leq 400$ by a simple χ^2 fit. We find that the 68% confidence limit for R marginalized over A is $1.50 \leq R \leq 1.63$ with $R = 1.57$ as best fit (see Fig. 13).

In Fig. 14 the confidence levels on R are translated to confidence levels in the $\Omega_\Lambda - \Omega_m$ plane which are then combined with the current SN1a results [40]. It is clear from this figure that the model can be brought in reasonable agreement with observations only if the universe is closed. The deviation from flatness becomes less and less important towards $\Omega_m \to 0$, where all the $R = $const lines converge at $\Omega_\Lambda = 1$. While the region with $\Omega_m > 1$ can be safely excluded from different cosmological observations, a moderately closed universe with $\Omega_\Lambda \sim 0.85$ and $\Omega_m \sim 0.4$ is compatible with supernova type Ia (SNIa) results and also with estimates for Ω_m from cluster abundance and x-ray data (see, e.g., Ref. [41]).
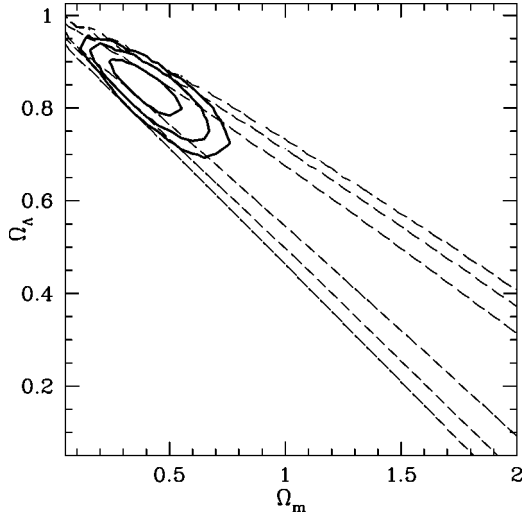
FIG. 14. The 68%, 95%, and 99% confidence levels for the cosmological parameters Ω_Λ and Ω_m, from the peak position detected by BOOMERanG and MAXIMA-1 for the model presented in this paper (dashed). The solid contours are obtained including the supernovae data.

As we have seen, the position of the first acoustic peak can be adjusted by choosing Ω_Λ and Ω_m so that the resulting universe is marginally closed. Nonetheless, the width of the peak, compressed by the increase of R, is still not in very good agreement with the data, as well as the isocurvature hump. The resulting normalized χ^2 is about ~ 1.8 for the best fit, which ''excludes'' the model at 70% confidence. One has however to keep in mind that the C_l's are not Gaussian and therefore the probability for our model to lead to the measured CMB anisotropies is even somewhat higher than 30%. In Fig. 15 two theoretical CMB spectra normalized to the COBE data are shown together with the MAXIMA-1 and BOOMERanG98 data. We did not optimize on the axion spectrum, or the baryon density parameter, but we chose $n_\sigma = 1.33$, $\Omega_m = 0.4$, and $\Omega_{baryon} = 0.05$.

Playing with the break-scale k_b we can in principle lower the second peak leaving the first one almost unchanged. Nevertheless, the position of the second peak is different from the one indicated by inflationary models and the data. Inter-
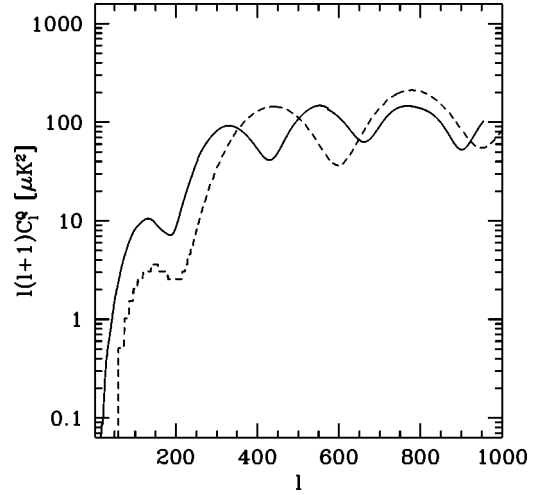

FIG. 16. The CMB polarization spectrum of our model (solid line) for the best fit parameters is compared with the inflationary CMB polarization spectrum in a critical universe with $\Omega_\Lambda = 0.7$. The fact that in our model the universe is closed is visible in the smaller distances between successive peaks.

peak distance is therefore a better estimator of the validity of a model. Clearly more and better data around the isocurvature hump region, i.e., $l \sim 100$, are needed to decide definitely whether the model is ruled out. This will most probably be achieved with the microwave anisotropy probe (MAP) satellite [42] planned for launch in 2001.

C. Polarization

The polarization spectrum distinguishes easily between adiabatic inflation and the axion seed model (see Fig. 16). The preferred closed universe for axion seeds translates into a smaller distance between polarization peaks. As the physical distance between peaks depends only on the sound speed, which is only slightly dependent on $\Omega_{baryon}h^2$, a quantity which is already tightly constrained by nucleosynthesis, the Δl on which this distance projects is mainly determined by spatial curvature, Ω_K [it depends also somewhat on Ω_Λ as can be seen from Eq. (4.5)], and is independent on the model for the initial fluctuations.
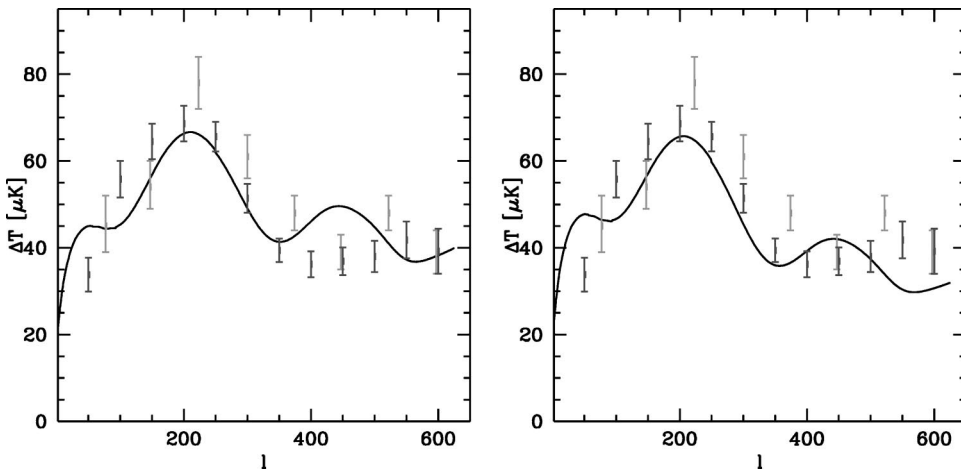

FIG. 15. Two theoretical CMB anisotropy spectra normalized to the COBE data, with $\Omega_\Lambda = 0.4$ and axionic spectral index $n_\sigma = 1.33$, are compared with the MAXIMA-1 and BOOMERanG98 data. From left to right, our model has a break at $k_b = 3/\eta_*$ and $k_b = 1/\eta_*$, respectively. Lowering k_b we subtract power on small scale and we can lower the second peak leaving the first one almost unchanged.
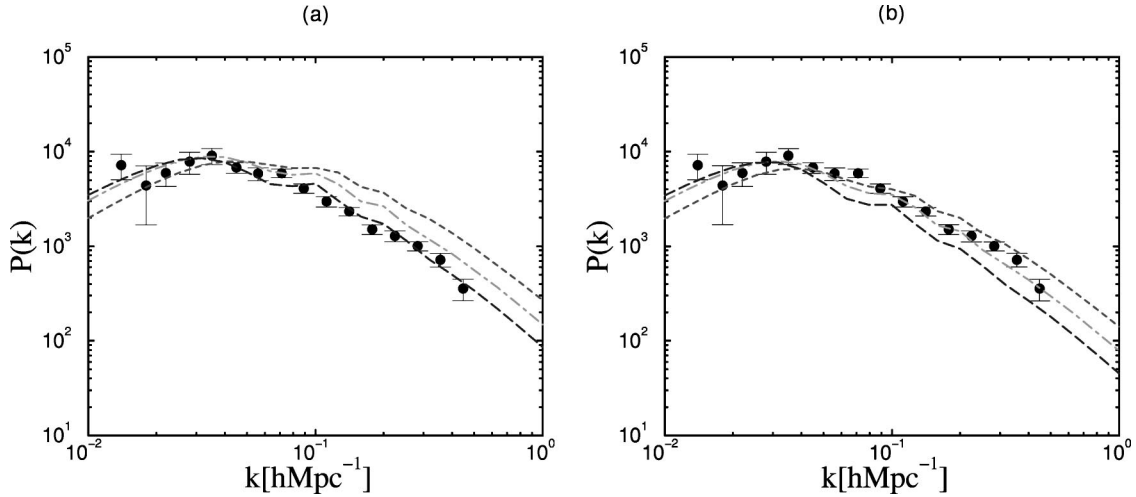
FIG. 17. The linear dark matter power spectra for fluctuations induced by axion seeds with spectral index $n_\sigma = 1.33$ and a break in the spectrum at (a) $k_b = 3/\eta_*$ and (b) $k_b = 1/\eta_*$, for a flat universe with $\Omega_m = 0.4$ (dotted), $\Omega_m = 0.3$ (dotted–dashed), and $\Omega_m = 0.25$ (dashed) are compared with data. We assume an IRAS galaxies bias of $b_I = \Omega_m^{-0.3}$.

D. The dark matter power spectrum

The computation of the dark matter power spectrum had already been performed in Ref. [25] where a considerable deviation from the data was found. In this work we repeat this computation taking into account the preferred values of the axion spectral index and of the matter energy density found from CMB data, and we introduce the break in the axion spectrum discussed above. With this additional input it is possible to establish reasonable agreement between the data and the dark matter power spectrum (see Fig. 17).

Since the computation of the theoretical matter power spectrum for a closed universe is relatively involved and since, for the purpose of comparing the theoretical spectrum with observations, we are interested in scales much below the curvature scale, we have computed it for a flat universe, with matter and a cosmological constant, assuming that the contribution from curvature is negligible on the scales under consideration. Indeed, what really plays a role for the matter power spectrum is the matter content, Ω_m, which fixes the time of equality between matter and radiation, determines when structures can start growing, and fixes the position of the bend in the power spectrum.

In Fig. 17 we present the theoretical dark matter power spectra together with the data as compiled by Peacock and Dodds [43]. Depending on the scale of the break in the axion spectrum, $\lambda_b = 1/k_b$, our model can be compatible with data for different values of Ω_m in the range $0.2 \lesssim \Omega_m \lesssim 0.4$. The role of the break is the following: if λ_b is small we subtract power only from small scales and we are able to reproduce a power spectrum in good agreement with data even if Ω_m is relatively high. However, if we do not introduce any break in the axion spectrum we find too much power on small scales and our theoretical dark matter power spectrum is incompatible with data (compare our present result with those found in Ref. [25]).

The root mean square mass fluctuation within a ball of radius $8h^{-1}$Mpc for the model with $n_\sigma = 1.33$, $k_b = 3/\eta_*$, and $\Omega_m = 0.25$ and for the model with $n_\sigma = 1.33$, k_b $= 1/\eta_*$, and $\Omega_m = 0.4$ are $\sigma_8 = 0.85$ and $\sigma_8 = 0.74$, respectively. Analysis of the abundance of galaxy clusters suggests $\sigma_8 \sim 0.5\Omega_m^{-0.5}$ [44].

E. Conclusions

We have shown that it is possible to choose cosmological parameters which bring our model in reasonable agreement with the present CMB anisotropy measurements, which is however less favorable than the striking fit of simple flat adiabatic inflationary models. This is our main result.

Even if our model will turn out to disagree with better data, we believe that we learn the important lesson that cosmological parameters obtained from CMB anisotropies are strongly model dependent, a point which is swept under the carpet by the vast majority of the circulating ''parameter-fitting'' literature. We believe that it is very important in the future to concentrate on model independent quantities, like interpeak distances, to determine cosmological parameters.

V. GRAVITATIONAL WAVES

Gravitational waves represent one of the most powerful tools to investigate the early history of the universe. They decouple at a temperature comparable to the string scale which makes them an important window for cosmological phenomena related to the string theory domain. In this section we show that axions can contribute substantially to the production of the gravitational wave background in the pre-big bang model, acting as a source in the tensor perturbation equation. This leads to a spectrum which is different from the standard gravitational wave background of string cosmology based on the ''direct mechanism'' of graviton production by amplification of quantum vacuum fluctuation. This new ''indirect mechanism'' leads to a flat spectrum and can easily be distinguished from the direct one. Indeed, as we shall see, the axion induced gravity wave background dominates the ''direct background'' at small frequencies and

represents an important observational constraint for string cosmology.

A. Direct production—Amplification of vacuum fluctuations

So far, amplification of quantum vacuum fluctuations have been considered as the principal mechanism for the production of gravitational waves during the pre-big bang phase [45–47]. During the dilaton era, before the big bang, when the scale factor evolves according to Eq. (2.9), the Fourier modes of metric tensor perturbations satisfy an evolution equation similar to Eq. (2.13), namely,

$$\ddot{\psi}_{\mathbf{k}}^T + \left(k^2 - \frac{\ddot{a}_T}{a_T} \right) \psi_{\mathbf{k}}^T = 0, \tag{5.1}$$

where $a_T = a e^{-\phi/2}$ is the pump field of gravity waves and $\psi_{\mathbf{k}}^T$ is the canonical variable for tensor modes of the metric. For the isotropic case discussed in this work, one find that $a_T \propto |\eta|^{1/2}$ independently on the evolution and number of dimensions during the pre-big bang phase. After proper normalization to the incoming vacuum, this yields the solution

$$\psi_{\mathbf{k}}^T = (-\eta)^{1/2} H_0^{(2)}(k\eta), \quad \eta < -\eta_1. \tag{5.2}$$

After the big bang, in the radiation dominated era, $\eta > \eta_1$, the solutions of Eq. (5.1) are simple plane waves. From the matching conditions between these two regimes, applying the same procedure as discussed in Sec. II B for the axion field, one obtains the following spectrum of gravitational waves,

$$\Omega_g \sim \frac{\omega_1^4}{H_0^2 m_{\text{Planck}}^2} \left(\frac{\omega}{\omega_1} \right)^3 \sim g_1^2 \left(\frac{\omega}{\omega_1} \right)^3 \Omega_\gamma, \tag{5.3}$$

which is a tilted spectrum, $\propto \omega^3$, normalized to g_1^2 at the string scale. One actually supposes that, at a string epoch $\eta_s < -\eta_1$, the dilaton-vacuum regime behavior of Eq. (2.9) breaks down and the universe undergoes a de Sitter expansion with linearly growing dilaton, which lasts until the beginning of the radiation dominated era η_1. This phase leads to a nearly flat gravitational wave spectrum at very small scales. The normalization of the spectrum to the string coupling g_1 can then be performed at a lower frequency, $\omega_s < \omega_1$, leading to a somewhat higher density of directly produced gravitons than the one discussed here. This is very important in order to make the direct background observable and still compatible with nucleosynthesis. (See Ref. [48] and references therein for more details.) A more detailed discussion on the important signatures and observational consequences of this direct production of gravitational waves can be found in Ref. [49] and references therein.

B. Indirect production—Axion source

Let us discuss now the production of a stochastic gravitational wave background generated by the presence of axion seeds. This indirect background will be superimposed to the direct one discussed above and will dominate the total spectrum at large scales. These two production mechanisms are fundamentally different. While the direct production of gravitons takes place during the pre-big bang phase and is due to the amplification of vacuum fluctuations, the indirect production is sourced by the axions during the post-big bang era.

The creation, propagation, and damping of gravitational waves in a Friedman background are described by the tensor perturbation equation (see, e.g., Ref. [50]),

$$\ddot{h}_{ij} + 2\frac{\dot{a}}{a}\dot{h}_{ij} - \Delta h_{ij} = 16\pi G a^2 \tau_{ij}, \tag{5.4}$$

where tensor perturbations in the metric are parametrized by the traceless, divergence-free, symmetric tensor field h_{ij},

$$g_{\mu\nu} = \bar{g}_{\mu\nu} + a^2(\eta) h_{\mu\nu}, \quad h_\mu^\mu = 0 = \nabla_\nu h_\mu^\nu, \tag{5.5}$$

which is a gauge invariant variable. As before a dot denotes the derivative with respect to conformal time. Equation (5.4) is a wave equation with source term τ_{ij}.

The tensor field h_{ij} is usually decomposed into two polarization states as

$$h_{ij}(\mathbf{x}, \eta) = h^\times(\mathbf{x}, \eta) \epsilon_{ij}^\times(\mathbf{x}) + h^+(\mathbf{x}, \eta) \epsilon_{ij}^+(\mathbf{x}), \tag{5.6}$$

where $\epsilon_{ij}^\times = \mathbf{e}_i^1 \mathbf{e}_j^1 - \mathbf{e}_i^2 \mathbf{e}_j^2$ and $\epsilon_{ij}^+ = \mathbf{e}_i^1 \mathbf{e}_j^2 + \mathbf{e}_i^2 \mathbf{e}_j^1$ are the polarization tensor fields and $(\mathbf{e}^1, \mathbf{e}^2, \mathbf{e}^3)$ is a local orthonormal basis (the wave is propagating in the $\mathbf{e}_3$ direction).

The energy density of gravitational waves is given by the 00 component of the energy momentum tensor of the wave. This can be defined as a space-average over several oscillations,

$$\rho_g = \frac{\langle \dot{h}_{ij} \dot{h}^{ij} \rangle}{16\pi G a^2} = \frac{\langle \dot{h}_\times^2 \rangle + \langle \dot{h}_+^2 \rangle}{16\pi G a^2}. \tag{5.7}$$

We decompose $h_\times$ and h_+ in Fourier modes,

$$h_\lambda(\mathbf{x}, \eta) = \int \frac{d^3k}{(2\pi)^3} e^{i\mathbf{k}\cdot\mathbf{x}} h_\lambda(\mathbf{k}, \eta), \quad \lambda = \times, +; \tag{5.8}$$

therefore

$$\dot{h}_\lambda(\mathbf{x}, \eta) = \int \frac{d^3k}{(2\pi)^3} e^{i\mathbf{k}\cdot\mathbf{x}} \dot{h}_\lambda(\mathbf{k}, \eta). \tag{5.9}$$

The spatial average then becomes

$$\langle \dot{h}_\lambda^2 \rangle = \int \frac{d^3k}{(2\pi)^3} \frac{d^3k'}{(2\pi)^3} e^{i\mathbf{x}\cdot(\mathbf{k}+\mathbf{k}')} \langle \dot{h}_\lambda(\mathbf{k}, \eta) \dot{h}_\lambda(\mathbf{k}', \eta) \rangle, \tag{5.10}$$

and we can use the stochastic average condition

$$\langle \dot{h}_\lambda(\mathbf{k}) \dot{h}_{\lambda'}(\mathbf{k}') \rangle = (2\pi)^3 \delta^3(\mathbf{k} - \mathbf{k}') \delta_{\lambda\lambda'} |\dot{h}_\lambda(\mathbf{k})|^2, \tag{5.11}$$

which yields, under the hypothesis of statistical isotropy,

$$\rho_g = \frac{1}{(\pi a)^2 16\pi G} \int dk\, k^2 |\dot{h}_\lambda(k, \eta)|^2. \tag{5.12}$$

We now compute the spectrum $|\dot{h}_\lambda(k,\eta)|^2$ in the coherent approximation. For this we introduce the deterministic source function $\Pi(k,\eta)$ defined by

$$4\pi G a^2 \Pi(k,\eta) \equiv \sqrt{H(k,\eta,\eta)}, \qquad (5.13)$$

[for the function H, see Eq. (2.68)]. The polarization tensors satisfy $\epsilon_{ij}^\lambda \epsilon_{\lambda'}^{ij} = 2\delta_\lambda^{\lambda'}$ and we can hence rewrite Eq. (5.4) in momentum space as

$$\ddot{h}_\lambda + 2\frac{\dot{a}}{a}\dot{h}_\lambda + k^2 h_\lambda = 8\pi G a^2 \Pi. \qquad (5.14)$$

The factor $1/2$ comes from the fact that Π sources both modes $\times$ and $+$ of h_{ij} and, assuming again statistical isotropy, each mode is sourced with the same strength. Since we want to compute a gravitational wave spectrum we only consider modes which enter the horizon in the radiation dominated era, $k\eta_* > 1$ and $\dot{a}/a \simeq 1/\eta$, the other modes being uninteresting (too large wavelength) for possible observations. Therefore we also consider modes far from COBE scale, $k \gg k_b$, and we can comfortably assume a flat axion spectral index, $n_\sigma = 1$. We then write Eq. (5.14) as

$$h_\lambda'' + \frac{2}{x}h_\lambda' + h_\lambda = \begin{cases} f(k)/\sqrt{x}, & x \leq 1 \quad \text{(active source)}, \\ 0, & x \geq 1 \quad \text{(dead source)}, \end{cases}$$
$$(5.15)$$

where the conformal time derivative has been replaced by the derivative with respect to $x = k\eta$. In this equation we assume that the axion source can be approximated by a power law behavior outside the horizon which is of the form

$$8\pi G a^2 \Pi(k,x) = x^{-1/2} k^2 f(k), \quad f(k) \simeq 8\pi g_1^2 k^{-3/2}, \qquad (5.16)$$

and can be considered negligible inside the horizon where the correlators decay quickly.

The homogeneous solutions to this equation are the spherical Bessel functions of index zero, $j_0(x)$ and $y_0(x)$. In the regime, $x \leq 1$, the solutions can be found with the Wronskian method, which yields

$$h_\lambda(k,x) = f(k)[c_1(x)j_0(x) + c_2(x)y_0(x)], \quad x \leq 1, \qquad (5.17)$$

where

$$c_1(x) = \int_0^1 dx\, x^{1/2}\cos x, \quad c_2(x) = \int_0^1 dx\, x^{1/2}\sin x, \qquad (5.18)$$

while in the second regime, $x \geq 1$, they are a linear combination of the homogeneous solutions,

$$h_\lambda(k,x) = A(k)j_0(x) + B(k)y_0(x), \quad x \geq 1. \qquad (5.19)$$

By matching Eqs. (5.17) and (5.19) at $x = 1$ we find

$$h_\lambda(k,\eta) = f(k)[c_1(1)j_0(k\eta) + c_2(1)y_0(k\eta)],$$

$$A(k) = f(k)c_1(1), \quad B(k) = f(k)c_2(1), \qquad (5.20)$$

which yields, for $x \gg 1$, $\dot{h}_\lambda \sim kh_\lambda \sim f(k)/\eta$, and thus

$$|\dot{h}_\lambda(k,\eta)|^2 \simeq \frac{(8\pi)^2 g_1^4}{\eta^2} k^{-3}. \qquad (5.21)$$

Using Eq. (5.12) we hence find

$$\rho_g = \frac{4g_1^4}{\pi G a^2 \eta^2}\int \frac{dk}{k} \quad \text{or} \quad \frac{d\rho_g}{d\log k} = \frac{4g_1^4}{\pi G a^2 \eta^2}, \quad (5.22)$$

which corresponds to a flat spectrum of gravitational waves.

On the other hand, at early time the radiation energy density, ρ_γ, dominates the Friedman equation which becomes

$$\frac{\dot{a}^2}{a^2} = \frac{8\pi G}{3}\rho_\gamma a^2. \qquad (5.23)$$

With $\dot{a}/a \simeq 1/\eta$ we can write the gravitational wave background spectrum produced by the axion field as

$$\Omega_g = \frac{\rho_g}{\rho_\gamma}\Omega_\gamma \sim 10 g_1^4 \Omega_\gamma. \qquad (5.24)$$

C. Observational consequences

In the preceding subsection we derived the spectrum of gravitational waves induced by axion seeds and we found that it is flat on scales much smaller than the COBE scale and normalized such as to lead to the correct amplitude of fluctuations in the CMB anisotropies.

Its normalization depends on the fundamental ratio between the string and Planck mass which is usually taken to be of the order of $g_1 \sim 0.1 \div 0.01$ [53]. The energy density of induced gravity waves is proportional to the fourth power of g_1 like the CMB anisotropy spectrum. Since the COBE normalization also depends on k_b [see Eq. (4.1)], which plays no rôle for the gravity wave spectrum on the scales considered here, g_1 alone is still allowed to vary in the range cited above even though Eq. (4.1) provides a precise constraint for a combination of g_1 and k_b. Using the previous values for g_1 we find a flat spectrum of gravity waves with $h^2\Omega_g \sim 4 \times (10^{-8} \div 10^{-12})$, a range which, most probably, will be reached by the third generation interferometers [51]. This renders the indirect gravity wave background an important observable of string cosmology. Note also that in the case of its detection it would provide a direct measurement of the string scale.

At present the most relevant observational bound for a gravity wave background comes from pulsars. In particular, the timing of the millisecond binary pulsar implies a limit on any stochastic gravity wave background of $h^2\Omega_g$ (at $f = 4.4 \times 10^{-9}$ Hz) $< 1 \times 10^{-8}$ (at 95% c.l.) [54], which transforms in our case into a limit on $g_1 \lesssim 0.07$ in this model.

The direct gravitational wave background has a blue spectrum and therefore dominates the indirect background on
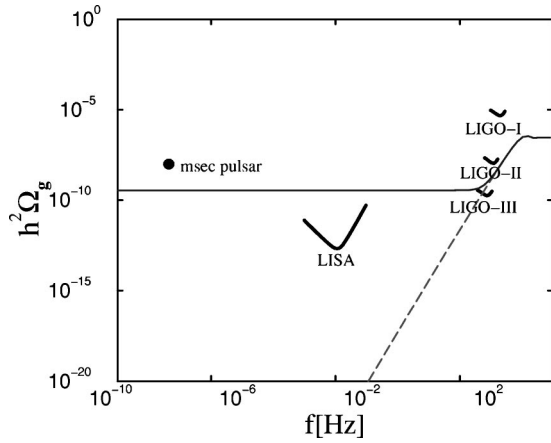
FIG. 18. The gravitational wave spectrum in pre-big bang model for a value of $g_1 = 0.03$. The directly produced background (dashed line) has been normalized to string mass at a frequency of $f_s = 500$ Hz. This frequency corresponds to the time $\eta_s = -1/(2\pi f_s a(\eta_0))$ for the transition between the dilaton-dominated regime and the de Sitter phase in the pre-big bang era (see above). The solid line represents the sum of the direct and indirect production of gravitational wave background. The analysis has been limited to frequencies $f \gg f_b$, where f_b denotes the frequency corresponding to the scale of the break.

small scales, as shown in Fig. 18.[4] The crossover frequency ω_c between the two regimes is determined by g_1 and the normalization frequency ω_s discussed above,

$$\omega_c = g_1^{2/3} \omega_s. \tag{5.25}$$

This crossover may actually, depending on the unknown value ω_s, fall into the range of frequencies at which interferometers will be operating.

Finally, we would like to point out that, like the CMB anisotropies of this model, the indirect gravity wave background considered here is not Gaussian, which can lead to interesting observational consequences.

VI. CONCLUSIONS

We have investigated the consequences of axion seeds which naturally occur in the context of string cosmology. We found that these seeds may induce the observed large scale

---

[4]Sensitivity curves for the Laser Interferometer Space Antenna (LISA) and Laser Interferometric Gravitational Wave Observatory (LIGO) are based on [51,52] and references therein. We acknowledge Carlo Ungarelli.

structure and CMB anisotropies in the universe provided that there is a break in the primordial axion power spectrum which from slightly blue on very large scales turns to a flat spectrum on scales smaller than the break, $k > k_b$. Such a break appears if the expansion law undergoes a transition during the pre-big bang phase. For the scenario to agree with observations the break must occur at $\eta_b \sim -0.3\eta_*$, which corresponds to an energy scale of the order of several GeV.

The axion seed model leads to isocurvature fluctuations with important contributions from vectors (about 50%) and tensors (about 15%) on large scales. The first acoustic peak in the CMB anisotropy power spectrum is around $l \sim 300$ for a flat model, $\Omega = \Omega_\lambda + \Omega_m = 1$. To reproduce observations the universe has to be closed with parameters, $\Omega_\Lambda \sim 0.85$ and $\Omega_m \sim 0.4$. This parameter choice is also in agreement with supernovae and cluster data. Even though our model leads to a larger χ^2 when fit to the CMB data it cannot be excluded by the presently available data. However, the ''isocurvature hump'' at $l \sim 40$ and the reduction not only of the second but also of the third acoustic peaks are signatures which clearly distinguish the model from standard inflationary scenarios. Furthermore the CMB polarization spectrum significantly differs from the inflationary result.

We have also studied gravitational waves which are generated during the post-big bang phase by the tensor type anisotropic stresses in the energy-momentum tensor of the axion field. We found that they lead to a flat observable background of gravity waves which can give stringent constraints on the model if detected by the planned LIGO-III and LISA observatories.

As the model studied is very predictive let us finally mention that its failure to reproduce observational data, which is hinted by present CMB anisotropy measurements and might be reinforced by future more accurate data, does not by itself rule out string cosmology. An additional important hypothesis of the model is that nongravitational interactions of the axion field with the dark matter may be neglected and the axion plays the role of a ''seed.'' If this hypothesis is relaxed, the axions may interact with radiation and dark matter and even lead to a standard adiabatic fluctuation spectrum. This idea deserves further study, but most probably the non-Gaussian character of the perturbations also survives in such a scenario.

---

[1] A. D. Miller *et al.*, Astrophys. J. Lett. **524**, L1 (1999).

[2] P. Mauskopf *et al.*, Astrophys. J. Lett. **536**, L59 (2000).

[3] P. de Bernardis *et al.*, Nature (London) **404**, 955 (2000).

[4] S. Hanany *et al.*, Astrophys. J. Lett. **545**, L5 (2000).

[5] L. Knox and L. Page, Phys. Rev. Lett. **85**, 1366 (2000).

[6] S. Dodelson and L. Knox, Phys. Rev. Lett. **84**, 3523 (2000).

[7] A. Melchiorri *et al.*, Astrophys. J. Lett. **536**, L63 (2000).

[8] M. Tegmark and M. Zaldarriaga, Phys. Rev. Lett. **85**, 2240 (2000).

[9] G. Veneziano, Phys. Lett. B **265**, 287 (1991); M. Gasperini

and G. Veneziano, Astropart. Phys. **1**, 317 (1993); Mod. Phys. Lett. A **8**, 3701 (1993); Phys. Rev. D **50**, 2519 (1994). An updated collection of papers on the pre-big bang scenario is available at http://www.to.infn.it/~gasperin/

[10] R. Brandenberger and C. Vafa, Nucl. Phys. **B316**, 391 (1989); Veneziano [9]; A. A. Tseytlin, Mod. Phys. Lett. A **6**, 1721 (1991); K. A. Meissner and G. Veneziano, Phys. Lett. B **267**, 33 (1991); Mod. Phys. Lett. A **6**, 3397 (1991); A. Sen, Phys. Lett. B **271**, 295 (1991); S. F. Hassan and A. Sen, Nucl. Phys. **B375**, 103 (1992); A. A. Tseytlin and C. Vafa, *ibid.* **B372**, 443 (1992); M. Gasperini and G. Veneziano, Phys. Lett. B **277**, 256 (1992).

[11] G. Veneziano, Phys. Lett. B **406**, 297 (1997); A. Buonanno *et al.*, Phys. Rev. D **57**, 2543 (1998).

[12] R. Brustein and G. Veneziano, Phys. Lett. B **329**, 429 (1994); N. Kaloper, R. Madden, and K. A. Olive, Nucl. Phys. **B452**, 677 (1995); Phys. Lett. B **371**, 34 (1996); R. Easther, K. Maeda, and D. Wands, Phys. Rev. D **53**, 4247 (1996); R. Easther and K. Maeda, *ibid.* **54**, 7252 (1996); M. Gasperini, J. Maharana, and G. Veneziano, Nucl. Phys. **B472**, 349 (1996); S. J. Rey, Phys. Rev. Lett. **77**, 1929 (1996); M. Gasperini and G. Veneziano, Phys. Lett. B **387**, 715 (1996); M. Gasperini, M. Maggiore, and G. Veneziano, Nucl. Phys. **B494**, 315 (1997); R. Brustein and R. Madden, Phys. Lett. B **410**, 110 (1997); Phys. Rev. D **57**, 712 (1988).

[13] M. S. Turner and E. J. Weinberg, Phys. Rev. D **56**, 4604 (1997); N. Kaloper, A. Linde, and R. Bousso, *ibid.* **59**, 043508 (1999); M. Maggiore and R. Sturani, Phys. Lett. B **415**, 335 (1997).

[14] J. E. Lidsey, D. Wands, and E. J. Copeland, Phys. Rep. **337**, 343 (2000).

[15] G. Veneziano, hep-th/0002094.

[16] D. A. Easson, hep-th/0003086.

[17] M. Gasperini and M. Giovannini, Phys. Lett. B **282**, 36 (1991); Phys. Rev. D **47**, 1519 (1993); Gasperini and Veneziano [9]; R. Brustein, M. Gasperini, M. Giovannini, V. F. Mukhanov, and G. Veneziano, Phys. Rev. D **51**, 6744 (1995).

[18] E. J. Copeland, R. Easther, and D. Wands, Phys. Rev. D **56**, 874 (1997); E. J. Copeland, J. E. Lidsey, and D. Wands, Nucl. Phys. **B506**, 407 (1997).

[19] A. Buonanno, K. A. Meissner, C. Ungarelli, and G. Veneziano, J. High Energy Phys. **01**, 004 (1998).

[20] R. Brustein and M. Hadad, Phys. Rev. D **57**, 725 (1998).

[21] R. Durrer, Phys. Rev. D **42**, 2533 (1990); Fundam. Cosm. Phys. **15**, 209 (1994).

[22] R. Durrer, M. Gasperini, M. Sakellariadou, and G. Veneziano, Phys. Lett. B **436**, 66 (1998).

[23] R. Durrer, M. Gasperini, M. Sakellariadou, and G. Veneziano, Phys. Rev. D **59**, 043511 (1999).

[24] M. Gasperini and G. Veneziano, Phys. Rev. D **59**, 048503 (1999).

[25] A. Melchiorri, F. Vernizzi, R. Durrer, and G. Veneziano, Phys. Rev. Lett. **83**, 4464 (1999).

[26] G. F. Smoot *et al.*, Astrophys. J. Lett. **396**, L1 (1992); C. L. Bennett *et al.*, *ibid.* **430**, 423 (1994).

[27] R. Brustein, M. Gasperini, and G. Veneziano, Phys. Lett. B **431**, 277 (1998).

[28] M. Gasperini, Phys. Rev. D **56**, 4815 (1997).

[29] C. Cartier, E. J. Copeland, and R. Madden, J. High Energy Phys. **01**, 035 (2000).

[30] C. Cartier and F. Vernizzi (in preparation).

[31] R. R. Metsaev and A. A. Tseytlin, Nucl. Phys. **B293**, 385 (1987).

[32] R. Durrer, M. Kunz, and A. Melchiorri, Phys. Rev. D **59**, 123005 (1999).

[33] N. Turok, Phys. Rev. D **54**, 3686 (1996).

[34] H. Kodama and M. Sasaki, Prog. Theor. Phys. Suppl. **78**, 1 (1984).

[35] R. Durrer and N. Straumann, Helv. Phys. Acta **61**, 1027 (1988).

[36] R. Durrer and M. Sakellariadou, Phys. Rev. D **56**, 4480 (1997).

[37] J. Magueijo, A. Albrecht, P. G. Ferreira, and D. Coulson, Phys. Rev. D **54**, 3727 (1996).

[38] W. Hu, D. Spergel, and M. White, Phys. Rev. D **55**, 3288 (1997).

[39] G. Efstathiou and R. J. Bond, Mon. Not. R. Astron. Soc. **304**, 75 (1999).

[40] S. Perlmutter *et al.*, Nature (London) **391**, 51 (1999).

[41] M. Roos and S. M. Harun-or-Rashid, astro-ph/0003040.

[42] See the MAP homepage at http://map.gsfc.nasa.gov/

[43] J. Peacock and S. Dodds, Mon. Not. R. Astron. Soc. **267**, 1020 (1994).

[44] V. Eke, S. Cole, and C. Frenk, Mon. Not. R. Astron. Soc. **282**, 263 (1996).

[45] M. Gasperini and M. Giovannini, Phys. Lett. B **282**, 36 (1992); Phys. Rev. D **47**, 1519 (1993).

[46] M. Gasperini and G. Veneziano, Phys. Rev. D **50**, 2519 (1994).

[47] R. Brustein, M. Gasperini, M. Giovannini, and G. Veneziano, Phys. Lett. B **361**, 45 (1995).

[48] A. Buonanno, M. Maggiore, and C. Ungarelli, Phys. Rev. D **55**, 3330 (1997).

[49] M. Gasperini, *String Theory in Curved Spacetimes* (World Scientific, Singapore, 1998), p. 333.

[50] C. W. Misner, K. S. Thorne, and J. A. Weeler, *Gravitation* (Freeman, San Francisco, 1973).

[51] M. Maggiore, Phys. Rep. **331**, 283 (2000).

[52] C. Cutler, Phys. Rev. D **57**, 7089 (1998).

[53] V. Kaplunovsky, Phys. Rev. Lett. **55**, 1036 (1985).

[54] S. Thorsett and R. Dewey, Phys. Rev. D **53**, 3468 (1996).